



Overview article

The segregation of transition metals to iron grain boundaries and their effects on cohesion

Han Lin Mai^a, Xiang-Yuan Cui^a, Daniel Scheiber^b, Lorenz Romaner^c, Simon P. Ringer^{a,*}^a School of Aerospace, Mechanical and Mechatronic Engineering & Australian Centre for Microscopy and Microanalysis, Faculty of Engineering, The University of Sydney, New South Wales 2006, Australia^b Materials Center Leoben Forschung GmbH, Roseggerstraße 12, Leoben 8700, Austria^c Department of Materials Science, University of Leoben, Franz-Josefstraße 18, Leoben 8700, Austria

ARTICLE INFO

Article history:

Received 22 November 2021

Revised 15 March 2022

Accepted 28 March 2022

Available online 2 April 2022

Keywords:

Segregation

Steel

Density functional theory

Grain boundaries

Cohesion

ABSTRACT

The segregation of transition metal elements to grain boundaries in steels plays a critical role in determining their cohesion. Here, we investigate the segregation, co-segregation, and cohesion effects of various transition metals (Co, Cr, Cu, Mn, Mo, Ni, Nb, Ti, V and W) to different grain boundary characters in ferritic-iron (α -Fe) through a systematic, brute-force style configurational analysis utilising density functional theory calculations. We demonstrate that differing grain boundary characters change not only transition metal segregation and co-segregation behaviours, but also their effects on cohesion. The effects of co-segregated solutes on cohesion can be substantially different from their summed individual parts. We show that solute-solute interactions at grain boundaries vary significantly as a function of grain boundary character. These interactions are shown to be substantially different from those that occur in the bulk. We introduce a novel quantitative method for assessing effects of segregated elements on interfacial cohesion through calculating the strength of bonds at a grain boundary in the DDEC6 bond-order framework. It is shown that work of separation quantities calculated through rigid separation of surfaces better captures the strength of bonding in most cases, and thus more accurately depicts intergranular fracture. Collectively, these results offer valuable insight towards rational grain boundary engineering in steels.

© 2022 The Author(s). Published by Elsevier Ltd on behalf of Acta Materialia Inc.

This is an open access article under the CC BY-NC-ND license

[\(<http://creativecommons.org/licenses/by-nc-nd/4.0/>\)](http://creativecommons.org/licenses/by-nc-nd/4.0/)

1. Introduction

Grain boundaries (GBs) are an important class of defects that play a significant role in the properties of engineering alloys. The control and engineering of GBs via thermomechanical processing, known as GB engineering [1], has attracted considerable attention as a method to control alloy properties. GB segregation refers to the presence of elevated concentrations of foreign elements accumulated near GBs. The segregation of either impurities and/or alloying elements to GBs has been shown to dramatically alter the cohesion of GBs [2,3]. It is also well known that GB character is a major factor in the determination of the segregation behaviour of different elements [4,5]. Importantly, various transition metals are often used in alloying to impart specific properties to the final al-

loy. The segregation of transition metals to GBs plays a key role in the stabilisation of nanocrystalline iron-based alloys [6,7]. Undesirable phenomena, such as temper embrittlement [8] and hydrogen embrittlement [9], mediated by GB segregation, can cause sudden catastrophic failure in the form of intergranular fracture in steels. Thus, understanding the segregation behaviour of transition metals to different types of GBs and their effects on cohesion is a prerequisite for knowledge-based GB engineering of steels with a resistance to such phenomena. However, behaviours that arise due to segregation effects can be difficult to isolate experimentally due to the complex nature of real alloys, despite recent advances [10,11]. To this end, many computational studies have focused on the elemental segregation of transition metal solutes to Fe GBs, and how they may affect GB cohesion [12–20]. However, such studies can contain seemingly conflicting information for even well-studied elements, as evidenced by a comprehensive review by Lejček et al. [21].

* Corresponding author.

E-mail address: simon.ringer@sydney.edu.au (S.P. Ringer).

In reality, the segregation of elements to GBs in alloys is complex, requiring careful consideration of the interplay between various effects. These effects range from those arising due to differing elemental behaviours, the chemical interactions with other segregating solutes, or distinct GB characters (i.e. local atomic geometry). The solute-solute interactions between segregating atoms at GBs are known as co-segregation effects. Such interactions can play a significant role in GB segregation behaviour, well reflected by the focus on such effects in steels for important solutes or impurities such as H [12,22–25], B and C [26], Zn [27], and P [14,24]. Regrettably, information on such co-segregation effects between pairs of segregating transition metals in steels remains scarce, and where they are studied, focus on specific cases e.g. Nb-X in Ref. [16] or Al and Si with Zn [27]. Therefore, a large swathe of the X-Y co-segregation space remains unexplored in steels, despite its importance in GB segregation, and hence cohesion. Pair-wise solute interactions between transition metals have previously been investigated in detail in bulk Fe [28]. However, these results cannot be reasonably extended to GBs, where significantly different local environments can alter such solute-solute interactions. Indeed, recent work on Mo [29] has found that interactions are almost exclusively repulsive at the GB, in stark contrast to the bulk where strong attractive interactions were observed. Thus, a deeper understanding of segregation phenomena can only be gained through thorough and systematic studies that explicitly address such co-segregation interactions, across a range of different GB archetypes. Importantly, how these co-segregation phenomena affect GB cohesion should also be assessed.

Here, we utilise density functional theory (DFT) to comprehensively investigate the segregation, co-segregation, and cohesion effects of the common substitutional alloying elements of Co, Cr, Cu, Mn, Mo, Ni, Nb, Ti, V and W in body-centred cubic (bcc) ferritic (α) Fe GBs. We chose to study these phenomena in four selected symmetric tilt coincident site lattice type bcc Fe GBs. These four GBs possess underlying structural features that represent the archetypes of: “twin-like/stacking fault” - $\Sigma 3(1\bar{1}2)[110]$, typical high-angle “coincident site lattice” - $\Sigma 3(\bar{1}\bar{1}1)[110]$, $\Sigma 11(3\bar{3}2)[110]$ and one that possesses characteristics of a low-angle tilt GB - the $\Sigma 9(2\bar{2}1)[110]$, due to the edge-dislocation core-like atomic structure at the interface [30]. Herein, they are referred to as $\Sigma 3(1\bar{1}2)$, $\Sigma 3(\bar{1}\bar{1}1)$, $\Sigma 11(3\bar{3}2)$ and $\Sigma 9(2\bar{2}1)$ for brevity. These GBs are formed from a range of typical structural units [30–32], allowing for an examination of segregation behaviours across a wide range of local atomic environments at the interface. Note that symmetric tilt GBs occur more commonly about the $<110>$ axis in polycrystalline Fe than others [30].

The structure of our study is as follows: First, we generated segregation profiles for the chosen solutes in the single-solute segregation cases in each of the four GBs. Second, the effects of each segregated solute on the cohesion of these GBs were calculated in the framework of Rice-Thomson-Wang's theory of interfacial embrittlement [33,34]. Third, the co-segregation and interaction effects of each of these solutes were investigated in an explicit, thorough brute-force style configurational analysis. This allowed the determination of all favourable co-segregating pairings and the interaction effects that occur between each of these segregating solutes at varying GB characters. Fourth, the cohesion effects of these co-segregating pairs at the GB were calculated and compared to the individual effects of each of these solutes, to determine whether the effects of certain solute pairings are greater than the sum of their parts. Finally, we utilised bond-order theory, as implemented in the DDEC6 framework [35], to quantitatively demonstrate a clear, positive, linear correlation between the summed bonding strengths of the bonds passing through a cleavage plane and the amount of work required to cleave the interface apart at that plane.

2. Methodology

We performed first principles calculations based on density functional theory (DFT) using the projector augmented wave (PAW) method [36] as implemented in the Vienna Ab-initio Simulation Package (VASP) [37,38]. Spin polarisation was accounted for in all calculations performed in this study. Various electronic exchange correlation functionals were tested, and the calculated lattice parameters, bulk moduli and magnetic moment are presented in the Supplementary Information (S.I.) in Supplementary Table S1. For this study, we utilised the generalised gradient approximation (GGA) via the Perdew-Burke-Ernzerhof (PBE) functional [39], as it generates values closest to those observed experimentally. The Brillouin-zone integrations for all GBs employed Monkhorst-Pack \mathbf{k} -point meshes, with an energy cut-off of 400 eV for the plane wave basis set. A first order Methfessel-Paxton scheme with a smearing width of 0.2 eV was adopted for all calculations. The convergence criterion for ionic force relaxation was set to below 0.01 eV/Å, and the criterion for total energy convergence in the electronic minimisation iterations was set to 1×10^{-5} eV. We utilised \mathbf{k} -point meshes of $6 \times 3 \times 1$, $6 \times 6 \times 1$, $6 \times 4 \times 1$ and $6 \times 6 \times 1$ for the $\Sigma 3(1\bar{1}1)$, $\Sigma 3(1\bar{1}2)$, $\Sigma 9(2\bar{2}1)$ and $\Sigma 11(3\bar{3}2)$ GBs, respectively. The choices of \mathbf{k} -point meshes and plane wave energy cutoff were checked with convergence tests, which are presented in the Supplementary Tables S5-S11.

2.1. Grain boundary structures

In this study, we chose to study the four symmetric tilt GBs, the $\Sigma 3(1\bar{1}1)[110]$, $\Sigma 3(1\bar{1}2)[110]$, $\Sigma 9(2\bar{2}1)[110]$ and $\Sigma 11(3\bar{3}2)[110]$ [Fig. 1]. The details regarding cell sizing and basic GB quantities such as excess volume, GB energy are presented in Table 1. In our construction of these GBs, atoms that were less than 0.7 times the bulk lattice vector apart in absolute distance were merged to become a single site, as to be consistent with the structures in Ref. [30]. This affects the $\Sigma 9(2\bar{2}1)[110]$ and $\Sigma 11(3\bar{3}2)[110]$ GBs. We constructed the GBs via the python package Atomic Simulation Environment [40]. The cells we built were all orthorhombic, with the exception of the $\Sigma 9(2\bar{2}1)[110]$, which was rhombic. The cells were constructed utilising the converged lattice vector as found in the functional testing, $a_0 = 2.832$. We did not allow the constructed cells to undergo cell-shape relaxation in the transverse direction (i.e. “a” and “b”, the in-GB plane directions). An optimisation of the “c” cell length (perpendicular to the GB plane) of the constructed supercell was performed in the calculations involving GB energies/excess volumes, which involve a cell without vacuum. In all other calculations, i.e. with vacuum, cell relaxations were not performed. The vacuum slab sizing was > 11 Å, in all non-cleaved cells in order to ensure exclusion of spurious surface-surface interactions. The relaxed GB structures in the vacuum cells are available as POSCAR files in the S.I. Atomic relaxations were performed in all calculations except those in the rigid-separation schemes.

2.2. Excess volume - V_{exc}

The excess volume of GBs is a standard quantity in GB characterisation that describes the amount of increased spacing around atoms at the GB interface compared to the bulk, useful for measuring the level of structural distortion that occurs at the GB. The quantity is defined per unit area of the interface as:

$$V_{\text{exc}} = (V_{\text{GB}} - N_{\text{GB}}/N_{\text{bulk}} \times V_{\text{bulk}})/(2A) \quad (1)$$

where V_{exc} is the excess volume, V_{GB} is the volume of the GB cell, V_{bulk} the volume of a similarly sized bulk cell, N_{GB} and N_{bulk} are the number of atoms in the GB and bulk cells, respectively.

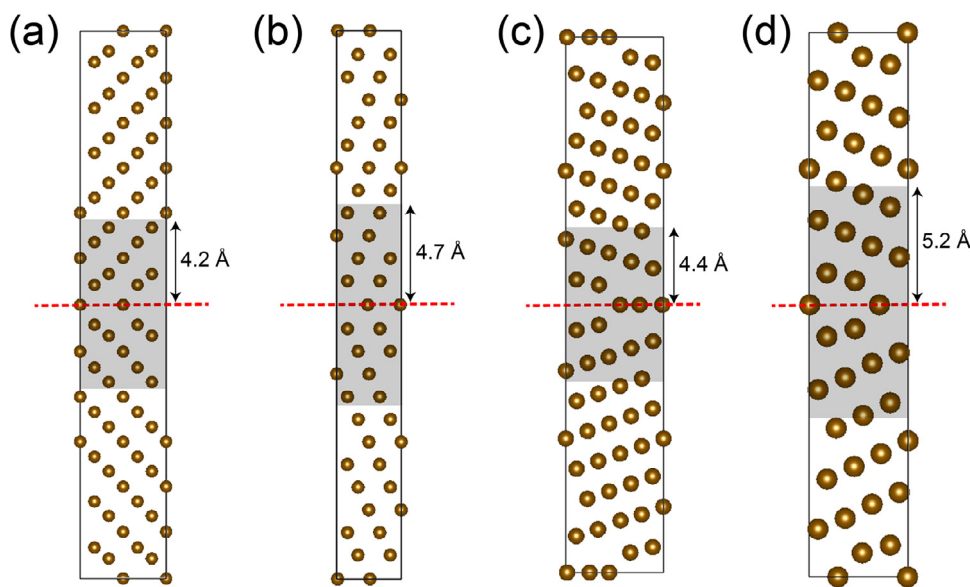


Fig. 1. The atomic structures of the four characteristic model GBs studied. The structures of the (1a) $\Sigma 3(1\bar{1}1)[110]$, (1b) $\Sigma 3(1\bar{1}2)[110]$, (1c) $\Sigma 9(2\bar{2}1)[110]$ and the (1d) $\Sigma 11(3\bar{3}2)[110]$ GBs, respectively. The GB interface planes are highlighted by the dashed red lines. The shaded ranges indicate the range of studied sites for segregation and co-segregation. The dimensions of these cells are given in Table 1. (For interpretation of the references to colour in this figure legend, the reader is referred to the web version of this article.)

Table 1

The sizes of the cells and number of atoms (n_{GB}) in them, and their corresponding GB quantities of excess volume (V_{exc}), GB energy (γ_{GB}) and work of separation (W_{sep}) are presented. Excess volume and GB energy calculations were conducted using GB cells without vacuum, i.e. as presented in Fig. 1. The smallest and largest sites by Voronoi volume, $V_{smallest}$ and $V_{largest}$, within 3 Å of the interface plane are presented. All other calculations in the study were conducted using the GB+vacuum cells.

System	n_{GB}	a (Å)	b (Å)	c_{GB} (Å)	$c_{GB} + \text{vac}$ (Å)	V_{exc} (Å)	$V_{smallest}$ (Å 3)	$V_{largest}$ (Å 3)	γ_{GB} (J/m 2)	W_{sep} (J/m 2)
$\Sigma 3(1\bar{1}1)[110]$	72	4.005	6.937	30.032	44.144	0.301	11.22	13.15	1.58	3.81
$\Sigma 3(1\bar{1}2)[110]$	48	4.005	4.905	27.995	41.620	0.124	11.45	11.83	0.45	4.72
$\Sigma 9(2\bar{2}1)[110]$	68	4.005	6.332	33.595	50.973	0.279	10.66	13.86	1.75	3.60
$\Sigma 11(3\bar{3}2)[110]$	42	4.005	4.696	25.838	50.973	0.240	11.24	13.05	1.45	3.83

Note that per-atom normalisation of the bulk term is necessary when merged sites are present in the constructed GB and hence contain fewer atoms than the corresponding bulk cell. The excess volumes of the GBs were carefully calculated by performing only the “c” length (direction perpendicular to the GB plane) optimisation, keeping the “a” and “b” lengths fixed (in the GB plane). The extension that resulted in the energetic minimum was used as the optimised GB cell for the calculation of the excess volume. These calculations for excess volume are performed on a cell containing two GB interfaces, i.e. without vacuum. The sizes of the final supercells are presented in Table 1. The detailed results involving these calculations are presented in the Supplementary Tables S12-16.

2.3. Grain boundary energy - γ_{GB}

The GB energy is the excess free energy that a GB possesses normalised per unit of interface area compared to the bulk crystal state of the parent material. The GB energy (γ_{GB}) is a key characteristic quantity that is often used to characterise GBs. The expression for γ_{GB} is given:

$$\gamma_{GB} = (E_{GB} - N_{GB}/N_{bulk} \times E_{bulk})/(2A) \quad (2)$$

where E_{GB} and E_{bulk} are the total energies of the cells containing a GB, and a bulk crystal of similar dimensions, respectively, and A the interfacial area present in the GB cell. The factor of two in the denominator is due to the periodic condition resulting in two GB interfaces present at the middle and top/bottom of the cell.

2.4. Cohesion quantities

2.4.1. Work of separation (rigid/relaxed) - W_{sep}

The Rice-Thomson-Wang model of thermodynamic interfacial embrittlement identifies the work of separation (W_{sep}) as a key quantity in the determination of fracture [33,34]. The work of separation of a GB may be expressed as a function of the cells containing a cleaved GB (i.e. with two free surfaces, separated at a specified cleavage plane) and a GB only:

$$W_{sep} = (E_{GB\text{-sep}} - E_{GB})/A \quad (3)$$

Note that the work of separation may also be computed as a function of the free surface energy (γ_{FS}). The free surface energy may be computed via:

$$\gamma_{FS} = (E_{bulk} - N_{slab}/N_{bulk} \times E_{slab})/(2A) \quad (4)$$

where E_{slab} is the energy of a slab cell with two free surfaces, each with area A. Then, the work of separation may be calculated using: $W_{sep} = 2\gamma_{FS} - \gamma_{GB}$.

There are two main methods of determining the work of separation in this study, and these are related to the mode of separation employed at a chosen cleavage plane with respect to the relaxation of the surfaces. We extensively tested all cleavage planes parallel to the GB plane. Diagrams depicting the chosen cleavage planes in each GB are presented in Supplementary Fig. S1. In the first method, relaxations of the surfaces formed by the cleaving of the grains are not performed. The quantity yielded by this method is the rigid work of separation, W_{sep}^{RGS} . This quantity is also known as the fracture energy. The second method, which allows for sur-

face relaxations in the cleaved grain cells, is the standard for determining the work of separation. This second quantity is denoted as W_{sep} . In this study, we use the *rigid* work of separation to determine the favourable cleavage plane, which is the plane that minimises the $W_{\text{sep}}^{\text{RGS}}$ required to cleave the grains. The cleaved structure at the plane that yielded the minimum $W_{\text{sep}}^{\text{RGS}}$ was then used to calculate the *relaxed* W_{sep} .

2.4.2. Sutton's ratio - R

Sutton's ratio [41] (R) is a measure of the likelihood of intergranular fracture occurring compared to transgranular fracture in brittle failure modes. Values of R close to or greater than 1 indicate that transgranular fracture is preferred, whereas lower values indicate a preference for intergranular fracture modes. It is calculated in the manner:

$$R = \frac{W_{\text{sep}}}{2\gamma_{\text{FS}}^{\text{PCP}}} \quad (5)$$

where $\gamma_{\text{FS}}^{\text{PCP}}$ is the free surface energy of the preferred cleavage plane in the bulk metal. In this study, we used the calculated free surface energy of the Fe (100) bcc surface of 2.50 J/m² for the quantity $\gamma_{\text{FS}}^{\text{PCP}}$, which has been suggested for bcc crystals [42].

2.4.3. Cohesion effect/cohesion change - η

The cohesion effect (η) of a solute may be quantified by the difference between the W_{sep} quantities with and without the segregated solutes. This term often goes by embrittling potency, or strengthening energy in other texts. However, the widespread use of these terms can prime readers for confusion, especially when the semantically signed and opposite terms "embrittling potency" and "strengthening energy" are used interchangeably. Using a semantically neutral term "cohesion effect" or "cohesion change" removes this ambiguity. In this work, it is calculated by:

$$\eta = W_{\text{sep}}^{\text{seg}} - W_{\text{sep}}^0 \quad (6)$$

where W_{sep}^0 and $W_{\text{sep}}^{\text{seg}}$ are the works of separation of the pure GB and the GB with segregated atoms, respectively. Negative values of η indicate that a solute has an embrittling effect, whereas positive values indicate that the solute has a cohesion enhancing effect on the GB.

2.5. Co-segregation study

The co-segregation study is detailed in the following. We studied two cases: where solute 1 is placed in the most energetically favourable site at the pure GB and is fixed in that site, and solute 2 is permuted around the GB decorated with solute 1, and vice versa. We refer to these structures herein as "ordered pair configurations". The most energetically favourable configuration in each ordered elemental pairing was selected for subsequent energetic and cohesion analysis. Where not specified herein, usage of the terms "configuration" or "case" refers to the minimum energy structure at an ordered pair.

This ostensibly neglects the possibility that the most energetically favourable configuration could have solutes occupying a site-combination that does not involve either solute at their most energetically favourable site in the pure-GB. However, in this study, most solute-solute interactions at the GBs are generally of small magnitude, and where they are significant, are mostly repulsive in nature. Note also the sharp dropoff in the magnitude of strength of segregation binding beyond the most favourable site [see Supplementary Figs. S2-5]. These combined factors of energetically repulsive solute-solute interactions with small segregation tendencies at other sites should render this possibility highly unlikely. Thus, it is reasonable to assume that our study accurately captures most of, if not all, of the minimum energy atomic configurations at the GB.

Here we remark that co-segregation interactions are generally important to study even if there are energetically competing mechanisms in the bulk [e.g. attractive solute-solute interactions in the bulk]. This is because elevated concentrations of solutes may be found near GBs that are not solely due to simple thermodynamic considerations of equilibrium segregation. These may include, but are not limited to, factors such as phase transformation and phase solubility considerations. These interactions may also play an important role in assessing kinetics-related segregation phenomena, such as how they may affect solute diffusion along GBs with prior-segregated solutes, or drive depletion/accretion mechanisms for certain solutes [e.g. [26]]. Nevertheless, we demonstrate in the Results section that the bulk solute-solute interactions for the solutes studied here are mostly negligible in terms of their impact on co-segregation.

2.6. Segregation

2.6.1. Segregation energy

Segregation energies represent the energy difference of a solute being situated at the GB compared to the bulk. The segregation energy (E_{seg}) of a substitutional solute X at any site is calculated with the following:

$$E_{\text{seg}} = E_{\text{GB}}[(n-1)\text{Fe}, X] - E_{\text{GB}} - [E_{\text{Bulk}}[(m-1)\text{Fe}, X] - E_{\text{Bulk}}] \quad (7)$$

where $E_{\text{GB}}[(n-1)\text{Fe}, X]$ is the total energy of a GB structure with n atoms containing a substitutional solute X, E_{GB} the total energy of the pure GB containing n Fe atoms, $E_{\text{Bulk}}[(m-1)\text{Fe}, X]$ the total energy of a bulk cell with m atoms containing a substitutional solute X, and E_{Bulk} the energy of that bulk cell in its pure form, containing m Fe atoms. The respective m and n for each case are presented in Table 1 and Supplementary Table S2. Here we use slab cells that possess the same dimensions as the GB to minimise the numerical errors associated with k-point sampling errors that occur due to different cell sizings [43].

A negative value indicate that a solute prefers to be situated at the GB compared to the bulk, i.e. *segregation*, with more negative values indicating stronger segregation tendencies. Positive values indicate anti-segregation, where a solute prefers the bulk to the GB environment. Importantly, these segregation energies may be used to determine real site-occupancy probabilities at the GB at some temperature and overall bulk solute concentration, by acting as inputs into the frameworks of various thermodynamic isotherm theories, e.g. those formulated by Langmuir-McLean [44] or White-Coghlan [45].

2.6.2. Incremental segregation energy

The incremental segregation energy ($E_{\text{seg}}^{\text{inc}}$) is used in this study to measure the likelihood of a second solute atom Y segregating to a GB that has been prior decorated with a segregated solute X. We calculated this quantity using:

$$E_{\text{seg}}^{\text{inc}} = E_{\text{GB}}[(n-2)\text{Fe}, X_i, Y_j] - E_{\text{GB}}[(n-1)\text{Fe}, X_i] - [E_{\text{Bulk}}[(m-1)\text{Fe}, Y] - E_{\text{Bulk}}] \quad (8)$$

where $E_{\text{GB}}[(n-2)\text{Fe}, X_i, Y_j]$ is the total energy of a GB containing substitutional solutes of element X and Y at sites i and j, respectively.

2.6.3. Total segregation energy

The total segregation energy can be used to assess the likelihood of a pair of solute atoms segregating to a particular grain boundary in absolute terms. We calculated this quantity using:

$$E_{\text{seg}}^{\text{total}} = E_{\text{GB}}[(n-2)\text{Fe}, X_i, Y_j] - E_{\text{GB}} - \left[E_{\text{Bulk}}[(m-1)\text{Fe}, X] + E_{\text{Bulk}}[(m-1)\text{Fe}, Y] - 2E_{\text{Bulk}} \right] \quad (9)$$

2.6.4. Interaction energy

The interaction energy is used in this study to quantify the magnitude and type of interaction that occurs between solute X and solute Y at the GB. This is calculated by:

$$E_{\text{int}} = E_{\text{GB}}[(n-2)\text{Fe}, X_i, Y_j] - E_{\text{GB}}[(n-1)\text{Fe}, X_i] - E_{\text{GB}}[(n-1)\text{Fe}, Y_j] + E_{\text{GB}} \quad (10)$$

Positive values indicate that this interaction is repulsive (i.e. energetically unfavourable), whereas negative values indicate that this interaction is attractive. If the sequential segregation of solute 2 is not favourable across all sites tested, then we quantify the interaction as the magnitude of the minimum segregation energy in the pure GB for solute 2 across all sites except the site occupied by solute 1. Then, this quantity is physically meaningful in the sense that we capture the size of the repulsive interaction that causes segregation of solute 2 to be unfavourable. In the case where sequential segregation is favourable, we capture the dynamics of whether these interactions encourage, discourage, or have no effect on sequential segregation.

2.6.5. Cohesion - configurational variation (ϵ_{config})

In this study we have computed two different configurations for any specific elemental combination. Let the combination be comprised of species X and Y. The corresponding configurational variation in the cohesion effect for this particular co-segregated elemental combination is:

$$\epsilon_{\text{config}} = \eta_{E-\text{min}}(\text{struct}[X, Y], \text{struct}[Y, X]) - \eta_{E-\text{max}}(\text{struct}[X, Y], \text{struct}[Y, X]) \quad (11)$$

where $\eta_{E-\text{min}}(\text{struct}[X, Y], \text{struct}[Y, X])$ and $\eta_{E-\text{max}}(\text{struct}[X, Y], \text{struct}[Y, X])$ are the cohesion changes in the structures with the minimum/maximum total energy between the X-Y (minimum energy structure where X is segregated first) and Y-X (minimum energy structure where Y is segregated first) structures. This quantity informs how large the variation in the computed cohesive effect at a combination would be between the two ordered configurations. Positive values indicate that the cohesion of the favourable configuration is higher than that of the less favourable one. Conversely, negative values indicate that the cohesion is worse in the favourable configuration. We do not compute ϵ_{config} in the cases where co-segregation in either X-Y or Y-X structures is unfavourable or unavailable (i.e. V-X, X-V cases in the $\Sigma 3(1\bar{1}2)$ GB). Additionally, we do not compute errors where either co-segregating configuration is less favourable than the single-element segregation configuration even if $E_{\text{seg}}^{\text{inc}} < 0$ in both cases.

2.6.6. Cohesion - heuristic error (ϵ_{heur})

In order to gain greater insight into the effects of co-segregation on cohesion compared to the commonly studied elemental (single atom) segregation, we computed a heuristic error quantity (ϵ_{heur}). This quantity measures the significance of the inclusion of co-segregation effects on a GB's cohesion. It was calculated by:

$$\epsilon_{\text{heur}} = \eta_{X,Y} - (\eta_X + \eta_Y) \quad (12)$$

where $\eta_{X,Y}$ is the cohesion change for a GB containing co-segregated species of both X and Y, and η_X, η_Y the cohesion changes of the GB containing only X and only Y, respectively. Positive values indicate that the combined effect of the co-segregated

solutes on GB cohesion is better than the summed individual effects (i.e. underestimated the cohesion in the co-segregated GB), and conversely, negative values indicate that the true cohesion is worse than estimated by the linear approximation (i.e. overestimated cohesion in the co-segregated GB).

We additionally computed the relative sizing of the heuristic error with respect to the true cohesion effect in an elemental combination:

$$\delta_{\text{heur}} = \frac{|\epsilon_{\text{heur}}|}{\eta_{X,Y}} \quad (13)$$

Note that to prevent the inclusion of cohesion effects with very small magnitudes that may occur in energetically favourable cases (i.e. $\eta_{X,Y} \approx 0$) from existing in the denominator, we excluded the cases where $|\eta_{X,Y}| < 0.1 \text{ J/m}^2$. In this manner, we only compute the relative errors in a linear approximation only where they are actually substantial in magnitude, to demonstrate these errors can be significant even when the true cohesion effect is substantial.

2.7. Bond orders

In this study, we have computed the electron density-derived bond orders utilising the DDEC6 framework [35]. We introduce a interface-specific quantity, the *area-normalised summed bond orders* in order to quantify the interface bonding strength. All the bonds that passed through each of the studied cleavage planes for both the single solute and co-segregation cases were identified. The sum of all bond orders of the bonds passing through a specific cleavage plane was calculated. For bonds extending into neighbouring cell images, we halve the corresponding bond order values. So, mathematically:

$$\sum_{\substack{\text{frac} \\ \text{path}}} \text{BO} = \sum_{i,j}^{i \neq j} \text{BO}[A_i, A_j] + \frac{1}{2} \sum_{k,l}^{k \neq l} \text{BO}[A_k, A_l] \quad (14)$$

where $A_1(z) < z_{\text{CP}} < A_2(z)$

where A_i, A_j, A_k, A_l are the atoms that are electronically bonded in sites i, j, k, l respectively, and A_1, A_2 represent the i, j and the k, l pairings in any order. A_i and A_j atoms reside entirely within the supercell created (i.e. bonds exist wholly within the cell), whereas A_k and A_l represent atom pairs where only one of A_k and A_l resides in the cell (i.e. possess bonds passing outside of the original cell into a neighbouring image). z_{CP} is the cleavage plane at z coordinate, for which the corresponding W_{sep} is also calculated.

3. Results

3.1. Grain boundary energies and excess volumes

When classifying GBs, it is useful to take note of the characteristic quantities known as GB energy and excess volume, whose computed values for the four model GBs are shown in Table 1. Both sets of values are in good agreement with previous studies [22,30] [Supplementary Table S4]. The $\Sigma 3(1\bar{1}1)$, $\Sigma 9(2\bar{2}1)$, $\Sigma 11(3\bar{3}2)$ GBs possess relatively larger excess volumes and GB energies compared to the stacking-fault/twin-like representative $\Sigma 3(1\bar{1}2)$ GB. This is in agreement with the results in Ref. [46], where they found higher levels of excess volumes tend to be correlated with higher GB energies. Higher GB energies generally indicate more significant distortions in the atomic structure at the interface, compared to the bulk.

3.2. Single solute segregation

The single solute segregation behaviours of the ten chosen transition metals were investigated by calculating their segregation en-

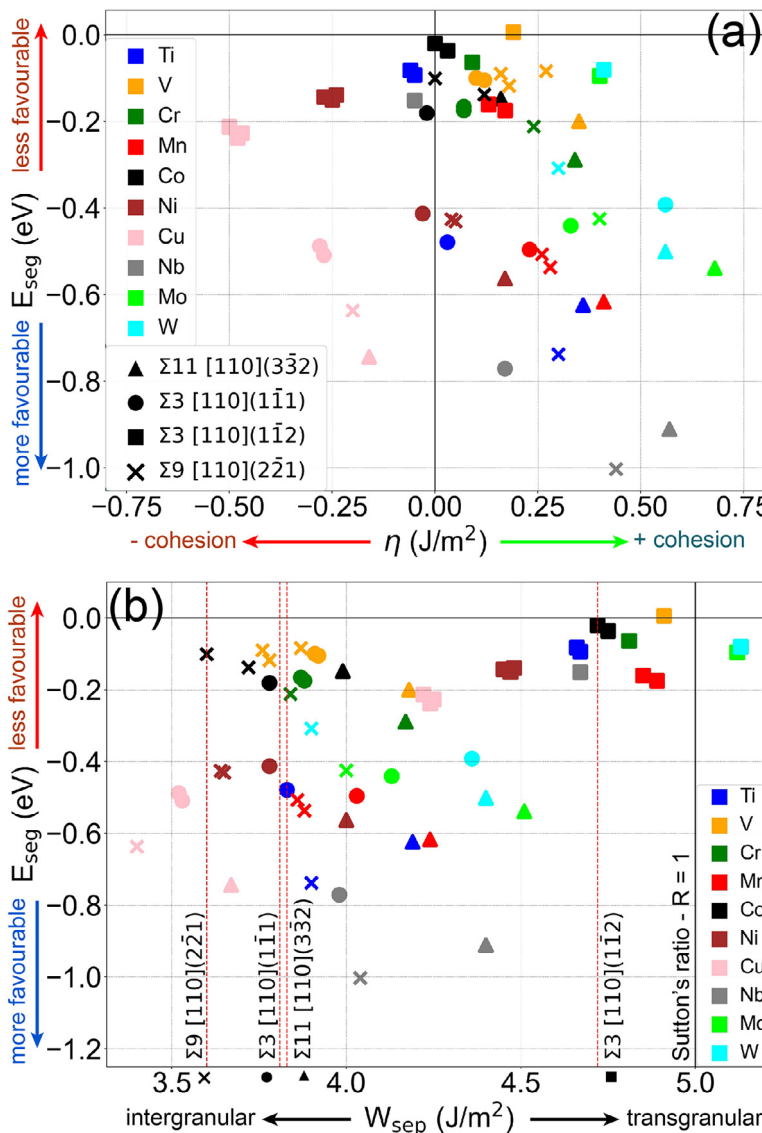


Fig. 2. The minimum segregation energy (E_{seg}), representative of tendency for a particular element to segregate to a GB, is plotted against their effects on GB cohesion when segregated (1 atom). (2a) The cohesion effect (η) that a segregated element has on the relaxed GB cohesion (Methods) is plotted against E_{seg} . (2b) The absolute cohesion, in the form of the work of separation (W_{sep}) of the GBs with the elements segregated is plotted against E_{seg} . The dotted red lines indicate the values of W_{sep} for the pure GBs. More negative energies of segregation represent a stronger tendency for the solute to be trapped in that particular GB. A reference line where Sutton's ratio at $R = W_{\text{sep}}/2\gamma_{\text{PCF}} = 1$ is plotted (see Methods). The data is available in Supplementary Tables S21-S24. (For interpretation of the references to colour in this figure legend, the reader is referred to the web version of this article.)

ergies (E_{seg}) at all available substitutional sites in the four characteristic GBs. The minimum segregation energies of the solutes to each of the four GBs are presented in Table 2 with literature comparisons, and plotted in Fig. 2. Comparisons with experimental segregation energies from the literature, where available, have been tabulated in the Supplementary Table S18. Note that such comparisons should generally be taken as qualitative, for reasons presented later in the Discussion. The zone of segregation trapping due to the presence of the GB extends no more than 3 Å normal to the interface plane, beyond which no significant segregation effects are observed. Our results for the segregation energies and cohesion effects are in agreement with the values from other studies, where available [15,23,47]. The element-wise specific segregation profiles at each GB are presented in Supplementary Figs. S2-5, data on the magnetic moments of the solutes in Supplementary Tables S29-33, and the relaxed Voronoi volumes at each solute site in Supplementary Tables S34-37. We plot the solute segregation energies

against the final relaxed Voronoi volumes at each site in Supplementary Figs. S6-15. The solute segregation energies are plotted against their magnetic moments in Supplementary Figs. S16-25. Their magnetic moments are also plotted against the final relaxed site Voronoi volume in Supplementary Figs. S26-35.

In Fig. 2, the role of GB character on single solute segregation may be seen. The significantly lower tendency of the stacking-fault/twin-type $\Sigma 3(1\bar{1}2)$ GB to trap solutes relative to the other GBs is immediately apparent. Note that the lower segregation binding is correlated with the significantly lower relative excess volume in the GB, which is often a distinguishing characteristic of twin/stacking-fault type GBs compared to random/general GBs. This is due to twin-like GBs being more bulk-like in structure at the interface than other GBs. The segregation energies tend to be somewhat similar across the $\Sigma 3(1\bar{1}1)$, $\Sigma 9(2\bar{2}1)$ and $\Sigma 11(3\bar{3}2)$ GBs, with an absolute maximum range in the segregation energy of ~0.26 eV across the three GBs for any single element. In this group

Table 2

The segregation energies present at the minimum energy site at the GBs studied (rotation axis [110] omitted for aesthetic purposes). Superscripts indicate the GB studied for that specific value: ^a - $\Sigma 3[110](\bar{1}\bar{1}1)$, ^b - $\Sigma 3[110](\bar{1}\bar{1}2)$, ^c - $\Sigma 9[110](\bar{2}\bar{2}1)$, ^d - $\Sigma 11[110](\bar{3}\bar{3}2)$, ^e - $\Sigma 5[100](013)$, ^f - $\Sigma 5[100](012)$, ^g - $\Sigma 5[100](010)$.

Element	E _{seg} (eV) - This work				Literature (see caption)
	$\Sigma 3(\bar{1}\bar{1}1)$	$\Sigma 3(\bar{1}\bar{1}2)$	$\Sigma 9(\bar{2}\bar{2}1)$	$\Sigma 11(\bar{3}\bar{3}2)$	
Co	-0.18	-0.04	-0.14	-0.15	-0.05 ^d [22], -0.09 ^{a,e} [16,22,47]
Cr	-0.18	-0.07	-0.21	-0.29	-0.03 ^a [22], -0.09 ^d [22], -0.13 ^a [19], -0.14 ^a [23], -0.18 ^a [17], -0.20 ^{a,e} [16,18,47], -0.24 ^f [19]
Cu	-0.51	-0.24	-0.64	-0.74	-0.26 ^e [16,47], -0.43 ^a [22], -0.57 ^a [18], -0.65 ^d [22]
Mn	-0.50	-0.18	-0.54	-0.62	-0.21 ^e [16,47], -0.32 ^a [22], -0.33 ^a [14], -0.44 ^{a,d} [22,23], -0.49 ^a [15], -0.50 ^e [12]
Mo	-0.44	-0.10	-0.43	-0.55	-0.37 ^e [16,47], -0.44 ^a [23], -0.61 ^a [48]
Nb	-0.77	-0.15	-1.00	-0.91	-0.49 ^e [16,47], -0.97 ^a [23]
Ni	-0.41	-0.15	-0.43	-0.56	-0.24 ^e [16,47], -0.31 ^a [22], -0.44 ^d [22]
Ti	-0.48	-0.09	-0.74	-0.65	-0.33 ^e [16,47], -0.39 ^a [22], -0.49 ^d [22], -0.52 ^a [23], -1.00 ^g [20]
V	-0.11	0.00	-0.12	-0.20	-0.18 ^e [16,47], -0.17 ^a [23], -0.12 ^a [48], -0.03 ^a [49], -0.04 ^d [22] 0.02 ^a [22],
W	-0.39	-0.08	-0.31	-0.51	-0.41 ^a [23], -0.49 ^a [18]

of GBs, the segregation tendency, in decreasing order, is roughly Nb > Cu > Ti, Mn > Ni, Mo, W > Cr, Co, V. In terms of variance of the minimum segregation energies in these three GBs, they may be separated into two groups, with Ti, Cu, Nb and W exhibiting large ranges across these GBs ($\Delta E_{seg}=0.26, 0.24, 0.23, 0.19$ eV) and V, Cr, Mn, Co, Ni, Mo exhibiting smaller ranges ($0.04 \leq \Delta E_{seg} \leq 0.12$ eV), with Ni sitting in the middle (0.15 eV). Importantly, this variance can change the ranking of segregation tendency of specific solutes between GBs. For example, Mn, Cr, V, Ni, Cu prefer to occupy $\Sigma 11(\bar{3}\bar{3}2) > \Sigma 9(\bar{2}\bar{2}1) > \Sigma 3(\bar{1}\bar{1}1) > \Sigma 3(\bar{1}\bar{1}2)$, whereas Nb and Ti prefer $\Sigma 9(\bar{2}\bar{2}1) > \Sigma 11(\bar{3}\bar{3}2) > \Sigma 3(\bar{1}\bar{1}1) > \Sigma 3(\bar{1}\bar{1}2)$.

3.3. Cohesion: Elemental segregation

The effects of each segregated solute on the cohesion of these GBs were then calculated using the work of separation (W_{sep}) quantity in Rice-Thomson-Wang's theory of interfacial embrittlement [33,34] [Fig. 2]. In Fig. 2a we present the change in GB cohesion (η) attributed to segregated atoms of each element for each GB, calculated in the relaxed separation framework. A similar plot for the rigid separation framework is presented in Supplementary Fig. S36. In Fig. 2b, an absolute measure of cohesion, in the form of W_{sep} is presented. We calculated the W_{sep} for each element in all substitutional sites that were within 0.05 eV of the minimum total energy in Fig. 2. There is generally good agreement with our calculated values of the cohesion effects, where data is available [Supplementary Tables S19, S20]. However, the comparison of these values is subject to certain conditions, which is an important but technical topic which is discussed in detail in a note in the S.I. In general, for purely elemental segregation, Mo and W are strong cohesion enhancers for all studied GBs, with Nb>Mn≈Ti>Cr>V≈Co in descending order for cohesion enhancement [Fig. 2a]. Ni can act as either a GB cohesion enhancer or an embrittler, depending on the GB to which it has segregated. Cu is an embrittler across all GBs studied, in agreement with the compiled results in Ref. [21]. Aside from Cu and Ni, we observe that the other transition metal solutes tend to range from non-factors in GB cohesion (e.g. Co) to strong enhancers of cohesion (e.g. Mo, W).

The results in Fig. 2 demonstrate that GB character not only affects the segregation tendencies of the transition metals, but also the induced cohesion effects. Note that the cohesion of the $\Sigma 3(\bar{1}\bar{1}2)$ GB is significantly higher compared to the other GBs, due to the nature of it being a twin GB, which closer resembles the bulk structure. However, it is also substantially more vulnerable to Cu embrittlement, which can render the W_{sep} below that of its peers with other elements segregated (e.g. $\Sigma 11(\bar{3}\bar{3}2)$ with Nb/Mo/W). The range of cohesion effects enacted on a GB by a segregated solute can vary significantly in magnitude. Elements such as Nb and Ti act as major cohesion enhancers in the $\Sigma 11(\bar{3}\bar{3}2)$, whereas their effects are negligible in the $\Sigma 9(\bar{2}\bar{2}1)$ and $\Sigma 3(\bar{1}\bar{1}1)$.

GBs. Additionally, note how W possesses a greater cohesion enhancing effect than Mo in the $\Sigma 3(\bar{1}\bar{1}1)$, but this is reversed in the $\Sigma 11(\bar{3}\bar{3}2)$. Both the $\Sigma 3(\bar{1}\bar{1}1)$ and $\Sigma 11(\bar{3}\bar{3}2)$ GBs may be classified as "high-angle" coincident site lattice GBs, and possess similar W_{sep} as pure GBs, but exhibit vastly different potentials for strengthening via segregation engineering for certain solutes (e.g. Cr, V, Nb, Mo). Overall, the $\Sigma 11(\bar{3}\bar{3}2)$ GB possesses a substantially higher potential for cohesion strengthening via elemental segregation, relative to the other GBs studied.

3.4. Co-segregation phenomena: Energetics

To investigate the likelihood of co-segregation, we calculated the incremental segregation energies (E_{seg}^{inc}) (Methods) of a second solute atom when the first is already segregated to the GB, situated in its most energetically favourable position [Table 3]. More negative values indicate that segregation binding of the second solute is stronger (i.e. more likely to occur). "N/A" values indicate that segregation of the second solute is unfavourable. The incremental segregation energies for each solute are plotted against their final relaxed Voronoi volume in Supplementary Figs. S38-47. The incremental segregation energies of the solutes are also plotted against their magnetic moments in Supplementary Figs. S48-57. Their magnetic moments are also plotted against the final relaxed site Voronoi volume in Supplementary Figs. S58-67. In this section, a sequence of four numbers given in parentheses (e.g. (a, b, c, d)), refer to a numerical breakdown for a specific property/statistic for the $\Sigma 3(\bar{1}\bar{1}1)$, $\Sigma 3(\bar{1}\bar{1}2)$, $\Sigma 9(\bar{2}\bar{2}1)$ and $\Sigma 11(\bar{3}\bar{3}2)$ GBs, respectively. Whilst it is not feasible to analyse all the data generated by our study on a case-by-case basis, there are several general trends that are highlighted as follows.

Prior to presenting results regarding the co-segregation energetics, it is important to also consider solute-solute interactions in the bulk. This is because attractive solute-solute interactions can potentially impede the segregation of solutes by trapping them in the bulk. To address this, we refer to the prior work performed by Gorbatov et al. [28], who demonstrated that such interactions between the transition metals in this study are almost exclusively negligible-repulsive in nature, with the only significant attractive interactions in the bulk occurring in the Cu-Cu case (-0.22 eV), Cu-Mn (-0.09 eV) and Cu-Ni (-0.08 eV). In general, these weak attractive interactions are not strong enough of a competing mechanism compared to the energetic reductions that occur due to segregation, except for the case of Cu segregation in the $\Sigma 3(\bar{1}\bar{1}2)$ GB, where the Cu-Cu attraction competes with the Cu-GB segregation energy reduction (-0.24 eV). As a result, the bulk solute-solute interactions may largely be neglected in their effect on interactive co-segregation, as studied here.

Of the 400 cases in Table 3, constituted of 100 ordered elemental pairings for each of the four GBs, there are 45 cases where

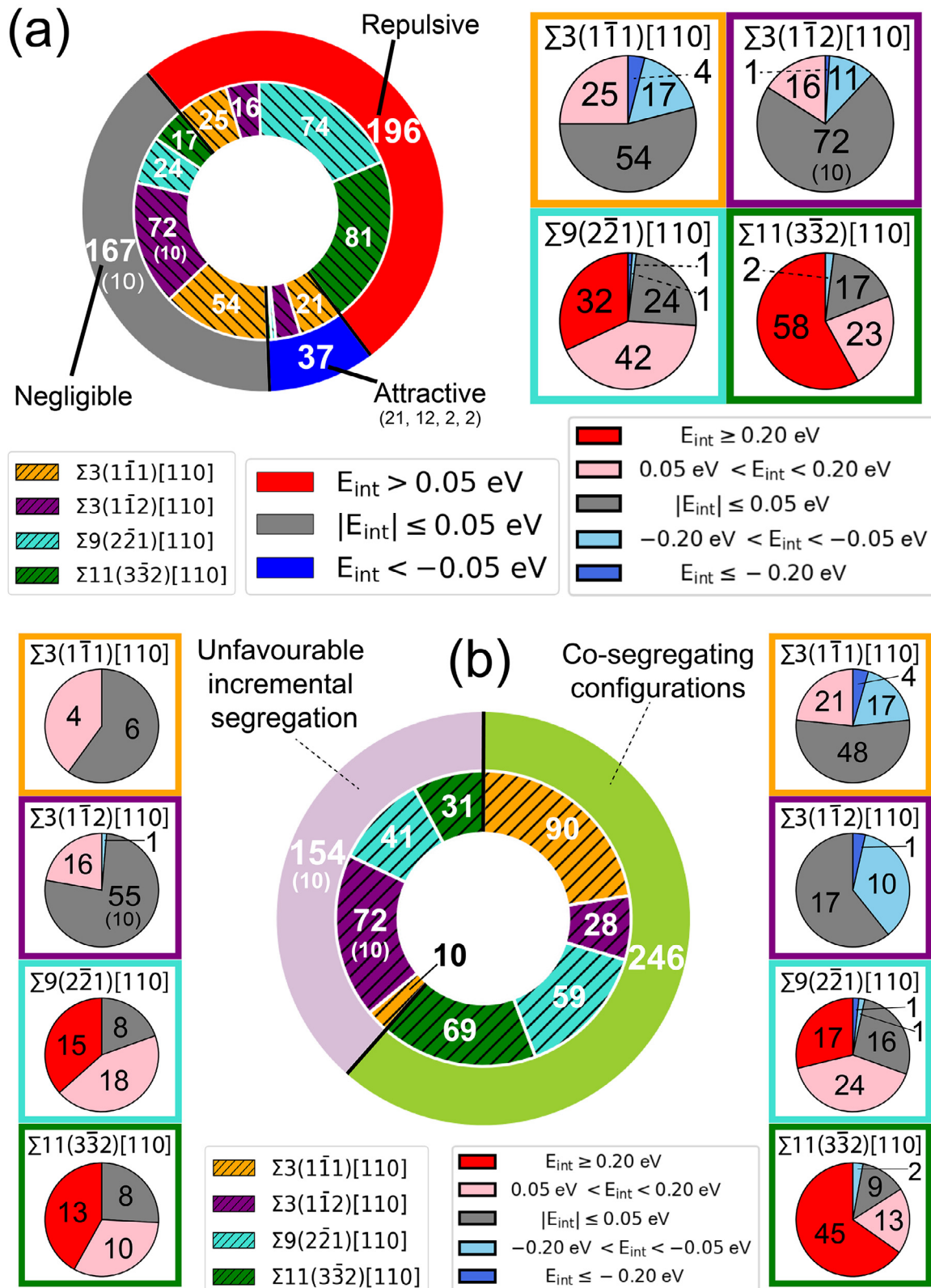


Fig. 3. An overall breakdown of the solute-solute interaction types and a distribution of interactions that occur in each GB. (3a) A breakdown of interactions that occur in all tested elemental-pair cases in the GBs studied are presented. The interactions in *all* studied cases in each GB are presented. (3b) The non co-segregating and co-segregating configurations are shown, and a breakdown of each GB's contribution to each of these classes are presented. Further breakdowns are provided of the type of interaction that occurs in each GB in both the unfavourable incremental segregation and co-segregating cases. The number in the brackets indicates that the number includes the 10 "V" cases not tested in the $\Sigma 3(1\bar{1}2)$, for completeness. The solute-solute interactions are classified as either negligible (grey), moderately repulsive (pink), strongly repulsive (red), moderately attractive (light blue), or strongly attractive (dark blue). (For interpretation of the references to colour in this figure legend, the reader is referred to the web version of this article.)

Table 3

The *incremental* energy of segregation ($E_{\text{seg}}^{\text{inc}}$) of solute 2 when solute 1 is present. Deeper shades of blue indicate a higher tendency to segregate for solute 2. The 45 (0, 25, 12, 8) "N/A" values, shaded in grey, indicate cases in which the segregation of solute 2 is unfavourable. The values shaded in yellow possess *incremental* $-0.1 \text{ eV} \leq E_{\text{seg}}^{\text{inc}} \leq 0 \text{ eV}$, which denote insignificant segregation tendencies (i.e. unlikely to occur). About one-third (154/400 - GB breakdown: 10, 72, 41, 31) of the considered co-segregation cases are therefore unlikely to occur in these GBs. The values in each cell correspond to the values for the $\Sigma 3(1\bar{1}\bar{1})$, $\Sigma 3(1\bar{1}2)$, $\Sigma 9(2\bar{2}\bar{1})$ and $\Sigma 11(3\bar{3}2)$ GBs, from top to bottom respectively. Copyable version in Supplementary Table S38.

Solute 1

Solute 2

	Ti	V	Cr	Mn	Co	Ni	Cu	Nb	Mo	W
Ti	-0.53	-0.11	-0.17	-0.48	-0.15	-0.39	-0.47	-0.93	-0.57	-0.50
	-0.05	-0.01	N/A	-0.01	-0.02	-0.17	-0.23	-0.15	-0.06	-0.05
	-0.10	N/A	-0.05	-0.35	-0.09	-0.33	-0.43	-0.14	-0.03	N/A
	-0.12	-0.04	-0.02	-0.10	-0.13	-0.51	-0.56	-0.31	-0.12	-0.04
V	-0.39	-0.08	-0.06	-0.38	-0.16	-0.38	-0.50	-0.62	-0.29	-0.23
	N/A									
	-0.13	0.00	-0.10	-0.37	-0.10	-0.38	-0.49	-0.29	-0.13	-0.05
	-0.34	-0.04	-0.04	-0.37	-0.10	-0.45	-0.54	-0.58	-0.24	-0.18
Cr	-0.47	-0.07	-0.14	-0.46	-0.09	-0.41	-0.49	-0.79	-0.43	-0.37
	N/A	N/A	N/A	-0.21	N/A	-0.12	-0.24	N/A	N/A	N/A
	-0.57	N/A	N/A	-0.32	-0.09	-0.43	-0.59	-0.79	-0.21	-0.08
	-0.26	N/A	N/A	-0.18	-0.07	-0.33	-0.44	-0.51	-0.25	-0.19
Mn	-0.46	-0.08	-0.13	-0.45	-0.13	-0.48	-0.56	-0.79	-0.45	-0.39
	-0.06	N/A	-0.09	-0.29	-0.02	-0.23	-0.34	-0.04	-0.08	-0.06
	-0.55	N/A	N/A	-0.34	-0.07	-0.39	-0.56	-0.76	-0.22	-0.09
	-0.12	N/A	N/A	-0.27	N/A	-0.24	-0.45	-0.40	-0.24	-0.13
Co	-0.45	-0.09	-0.13	-0.44	-0.18	-0.41	-0.53	-0.71	-0.34	-0.29
	-0.08	-0.02	-0.02	-0.14	-0.03	-0.14	-0.26	-0.09	-0.01	-0.02
	-0.69	-0.08	-0.15	-0.48	-0.09	-0.44	-0.66	-0.93	-0.34	-0.21
	-0.60	-0.15	-0.20	-0.47	-0.17	-0.54	-0.68	-0.84	-0.42	-0.39
Ni	-0.45	-0.09	-0.17	-0.56	-0.18	-0.40	-0.73	-0.71	-0.33	-0.26
	-0.11	N/A	-0.03	-0.26	-0.02	-0.23	-0.39	-0.12	-0.01	N/A
	-0.64	-0.07	-0.14	-0.49	-0.13	-0.45	-0.68	-0.87	-0.30	-0.18
	-0.58	-0.09	-0.07	-0.29	-0.12	-0.38	-0.53	-0.76	-0.32	-0.26
Cu	-0.44	-0.09	-0.16	-0.55	-0.18	-0.46	-0.74	-0.70	-0.32	-0.24
	-0.09	0.00	-0.06	-0.28	-0.06	-0.28	-0.52	-0.17	-0.07	-0.03
	-0.54	-0.08	-0.19	-0.47	-0.16	-0.48	-0.63	-0.75	-0.16	-0.03
	-0.44	-0.04	-0.04	-0.26	-0.09	-0.35	-0.64	-0.58	-0.18	-0.07
Nb	-0.62	-0.17	-0.20	-0.51	-0.12	-0.36	-0.45	-1.03	-0.65	-0.57
	-0.05	N/A	N/A	-0.07	N/A	-0.13	-0.25	-0.17	-0.02	-0.01
	-0.03	N/A	N/A	-0.30	-0.07	-0.30	-0.38	-0.03	N/A	N/A
	-0.07	-0.02	N/A	-0.11	-0.08	-0.41	-0.41	-0.12	-0.01	0.00
Mo	-0.61	-0.14	-0.17	-0.50	-0.08	-0.30	-0.44	-0.97	-0.58	-0.50
	0.00	N/A	N/A	-0.19	N/A	-0.06	-0.22	N/A	N/A	N/A
	-0.09	N/A	-0.05	-0.33	-0.05	-0.31	-0.37	-0.23	-0.10	-0.03
	-0.21	-0.02	N/A	-0.32	-0.03	-0.34	-0.38	-0.35	-0.18	-0.11
W	-0.59	-0.11	-0.15	-0.50	-0.07	-0.28	-0.46	-0.95	-0.55	-0.46
	-0.02	N/A	N/A	-0.16	N/A	-0.04	-0.18	-0.09	N/A	N/A
	-0.08	N/A	-0.06	-0.32	-0.04	-0.30	-0.34	-0.22	-0.09	-0.02
	-0.16	-0.01	N/A	-0.24	-0.04	-0.33	-0.31	-0.30	-0.14	-0.07

Incremental $E_{\text{seg}}^{\text{inc}}$ (eV)

co-segregation is completely unfavourable [i.e. $E_{\text{seg}}^{\text{inc}} = 0 \text{ eV}$], excluding the 10 V-X cases dropped due to initially positive E_{seg} of V in the $\Sigma 3(1\bar{1}2)$. Cases where incremental segregation is completely unfavourable are shaded in grey in Table 3. Note all pairings for the $\Sigma 3(1\bar{1}\bar{1})$ GB are favourable for co-segregation. However, many of the remaining incremental energies of segregation are only slightly negative, resulting in a negligible likelihood of binding to the GB. Thus, such cases are phenomenologically unin-

teresting. Therefore, we extend our criterion to include such cases, qualified where $E_{\text{seg}}^{\text{inc}} > -0.1 \text{ eV}$, resulting in 154 cases that exhibit negligible co-segregation. Segregation energies that satisfy such a threshold still yield extremely low probabilities of segregation at finite temperatures [Supplementary Fig. S37]. These cases are highlighted in yellow in Table 3. For the sake of semantics, we describe cases that fulfil such conditions as possessing "unfavourable incremental segregation" in the remaining text.

Table 4

The interaction energies (E_{int}) that occur between the solutes at the GBs. The presented quantity is calculated at the minimum energy configuration for solute 2 when solute 1 is already present as the first segregated atom, at its most favourable site. Blue indicates attractive interactions (negative), red repulsive (positive). "N/A" values, shaded in grey, were not calculated since the segregation of "V" to the $\Sigma 3(1\bar{1}2)$ as solute 1 is unfavourable. Values suffixed with "*" indicate that this is a case with an incremental energy of segregation that results in physically insignificant co-segregation of solute 2, and "+" indicates that co-segregation of solute 2 is completely unfavourable. The values in each cell correspond to the values for the $\Sigma 3(1\bar{1}1)$, $\Sigma 3(1\bar{1}2)$, $\Sigma 9(2\bar{2}1)$ and $\Sigma 11(3\bar{3}2)$ GBs, from top to bottom respectively. Copyable version in Supplementary Table S39.

Solute 1

Solute 2

	Ti	V	Cr	Mn	Co	Ni	Cu	Nb	Mo	W
Ti	-0.05 0.04* 0.19* 0.51	-0.01 -0.03* 0.09+ 0.03*	0.01 0.07+ 0.12* 0.05*	0.01 0.17* 0.19 0.51	0.03 0.02* 0.04* 0.02	0.02 -0.03 0.10 0.05	0.04 0.01 0.21 0.19	-0.15 -0.03 0.43 0.61	-0.13 -0.02* 0.28* 0.42	-0.11 -0.04* 0.25+ 0.46*
V	0.09 N/A 0.16 0.30	0.03* N/A 0.09* 0.03*	0.11* N/A 0.06* 0.24*	0.12 N/A 0.17 0.23	0.02 N/A 0.04* 0.03*	0.03 N/A 0.05 0.12	-0.01 N/A 0.15 0.20	0.15 N/A 0.29 0.33	0.15 N/A 0.19 0.31	0.16 N/A 0.20* 0.33
Cr	0.01 0.09+ 0.17 0.37	0.03* 0.00+ 0.12+ 0.20+	0.03 0.07+ 0.16+ 0.28+	0.04 -0.05 0.19 0.02	0.09* 0.04+ 0.01* 0.06*	0.01 0.02 0.00 0.23	0.02 -0.01 0.05 0.31	-0.02 0.12+ 0.22 0.40	0.01 0.07+ 0.21 0.30	0.02 0.03+ 0.23* 0.32
Mn	0.02 0.00* 0.19 0.51	0.02* 0.00+ 0.12+ 0.20+	0.04 -0.06* 0.16+ 0.28+	0.05 -0.12 0.17 -0.06	0.05 -0.01* 0.03* 0.14+	-0.07 -0.07 0.03 0.32	-0.07 -0.12 0.08 0.06	-0.05 -0.12 0.24 0.51	-0.02 0.04* 0.21 0.31	0.00 -0.05* 0.21 0.37
Co	0.03 0.02* 0.04 0.02	0.01* 0.04* 0.04* 0.04	0.04 -0.03* 0.01 0.08	0.05 0.02 0.16+ 0.28+	0.00 0.04* 0.01* -0.04	0.00 -0.01 -0.01 0.02	-0.04 -0.02 -0.02 0.06	0.06 0.07* 0.07 0.07	0.10 -0.03* 0.09 0.13	0.11 -0.03* 0.10 0.11
Ni	0.03 -0.03 0.10 0.05	0.02* 0.00+ 0.05* 0.10*	0.01 0.00* 0.02 0.21	-0.07 -0.10 -0.08 0.32	0.00 0.00* -0.08 0.00	0.01 -0.09 -0.03 0.18	-0.59 -0.16 -0.04 0.22	0.06 0.00 0.13 0.15	0.11 0.03* 0.13 0.23	0.13 0.03+ 0.07 0.24
Cu	0.04 0.00* 0.20 0.19	0.01* -0.02* 0.01* 0.03*	0.02 -0.03* -0.03 0.11*	-0.05 -0.12 -0.02 0.35	0.00 -0.02* -0.02 0.04*	-0.05 -0.14 -0.05 0.21	-0.60 -0.28 -0.05 -0.13	0.08 -0.05 0.27 0.33	0.12 -0.04* 0.27 0.37	0.16 -0.04* 0.22* 0.43*
Nb	-0.14 0.01* 0.26* 0.59*	-0.07 0.00+ 0.09+ 0.05*	-0.02 0.07+ 0.21+ 0.29+	-0.02 0.09* 0.24 0.51	0.06 0.04+ 0.07* 0.07*	0.05 0.01 0.13 0.15	0.06 -0.02 0.26 0.33	-0.26 -0.09 -0.21 0.79	-0.21 -0.02* -0.18 0.56*	-0.18 -0.01* 0.25+ 0.09*
Mo	-0.13 0.02* 0.20* 0.42	-0.04 0.00+ 0.09+ 0.06*	0.01 0.07+ 0.11* 0.07+	-0.01 -0.03 0.21 0.30	0.11* 0.04+ 0.09* 0.00*	0.11 0.08* 0.13 0.22	0.04 0.01 0.27 0.36	-0.20 0.12+ 0.35 0.56	-0.14 0.07+ 0.21 0.37	-0.10 0.03+ 0.22* 0.39
W	-0.11 0.03* 0.20* 0.46	-0.01 0.00+ 0.09+ 0.06*	0.02 0.07+ 0.10* 0.29+	0.00 0.00 0.22 0.37	0.11* 0.04+ 0.10* 0.11*	0.13 0.04+ 0.14 0.24	0.03 0.05 0.18 0.43	-0.18 -0.01* 0.35 0.62	-0.11 0.07+ 0.23* 0.40	-0.07 0.03+ 0.23* 0.43*

Interaction energy (eV)

The corresponding interactions that occur between the solutes at the most energetically favourable configuration in each ordered pair are presented in [Table 4](#), quantified by the energy of interaction (E_{int}) (Methods). Positive (negative) values of E_{int} indicate that the segregation of solute 2 is discouraged (encouraged) by solute 1. We classify these interactions as *repulsive* where $E_{\text{int}} > 0$ eV and *attractive* where $E_{\text{int}} < 0$ eV. In the remaining text, for ease of reading, we class these interactions by magnitude, *negligible* where

$|E_{\text{int}}| \leq 0.05$ eV and *significant* where $|E_{\text{int}}| > 0.05$ eV, which we further classify into *moderate* where $0.05 < |E_{\text{int}}| < 0.2$ eV, and *major* in the case where $|E_{\text{int}}| \geq 0.2$ eV [for justification, see S.I.]. A breakdown of the interaction types occurring as a function of GB is presented in [Fig. 3a](#). The types of interactions occurring in all cases are further divided into categories where co-segregation is favourable and unfavourable in [Fig. 3b](#). Lastly, note that the large majority of interactions tend to be negligible or repulsive [[Fig. 3a](#)].

We first examined GB character and its influence on sequential segregation [Table 3, Fig. 3a]. The number of cases with unfavourable incremental segregation in each GB appears to be roughly inversely correlated with the excess volume present. The stacking-fault/twin-like $\Sigma 3(1\bar{1}2)$ is responsible for a disproportionate number of elemental pairs which result in unfavourable incremental segregation. The small magnitudes of interaction energies [Fig. 3a] indicate that the sites available for segregation in the $\Sigma 3(1\bar{1}2)$ GB generally tend to have poor binding and/or are few in number. This causes even small repulsive interactions to be sufficient to retard segregation completely, or even attractive interactions to be insufficient to encourage significant co-segregation, due to the originally weak segregation binding at the GB. Note specifically the dependency of interaction behaviours between large solutes (i.e. Ti, Nb, Mo, W) on GB character, ranging from attractive in the $\Sigma 3(1\bar{1}1)$, or significantly repulsive in the $\Sigma 9(2\bar{2}1)$ and $\Sigma 11(3\bar{3}2)$.

We then examined the influence of local atomic structure at a GB on co-segregation [Fig. 3b]. Configurations which involve significant repulsive interactions predominantly feature in either the $\Sigma 9(2\bar{2}1)$ or $\Sigma 11(3\bar{3}2)$ GBs. This implies that their local atomic structures allow for strong segregation binding in the pure GB, but also discourages segregation beyond the first atom due to repulsive interactions. This is a result of their local atomic structure being significantly different to the $\Sigma 3(1\bar{1}1)$ GB despite their similar excess volumes, discussed in detail in Ref. [30]. However, these major repulsive interactions fail to completely discourage co-segregation in a large majority of these cases. It may then be inferred that sites which bind solutes strongly without inducing the large repulsive interactions generally do not exist in either GB. Such sites should, in theory, out-compete the sites where strong repulsive interactions occur. In contrast, most interactions in the $\Sigma 3(1\bar{1}1)$, which has a similar excess volume to these two GBs, range from negligible to significantly attractive. In this case, it may be understood that the $\Sigma 3(1\bar{1}1)$ GB possesses a local structure that intrinsically can accommodate more solutes per unit area by minimising significant repulsive interactions. This is reflected by the high proportion of the cases that qualify as co-segregating in this GB, relative to the others.

The trends of co-segregation were then considered on an elemental basis. There are two groups of elements, V/Cr/Co and Nb/Mo/W, which together participate in 149 of the 154 cases where unfavourable incremental segregation occurs. V/Cr/Co partakes in 107 of the 154 of these cases. Nb/Mo/W participates in 79 of the 154 of these cases. V, Cr and Co exhibit very weak segregation binding even in the pure GBs. Therefore, the origins of their representation can be understood to arise from the weak segregation binding that these solutes exhibit in Fe GBs. On the other hand, the rejection of co-segregation where Nb, Mo and W are involved cannot be understood in this manner, as they exhibit considerably strong segregation tendencies to pure GBs. The origin of these effects is related to the *misfit* of these atoms with respect to the Fe-lattice. Weakly segregating elements, such as V/Cr/Co are “crowded out” by partner elements that either bind stronger to the favourable sites (i.e. site competition) and/or are repelled by interactions with the already-present prior segregants such that segregation becomes unfavourable. Larger elements, in the cases of the Nb/Mo/W atoms, tend to become unfavourable due to a lack of strongly binding segregation sites i.e. in the $\Sigma 3(1\bar{1}2)$, or due to the repulsive interactions between large atoms, i.e. in the $\Sigma 9(2\bar{2}1)/\Sigma 11(3\bar{3}2)$ GBs. This is evidenced by the number of cases where co-segregation when any of Nb, Mo and W is the first atom present at the GB, which accounts for 56 of the 79 cases where unfavourable incremental segregation occurs involving Nb/Mo/W.

It is informative to consider a breakdown of the interactions that occur in the unfavourable incremental segregation and co-

segregating cases [Fig. 3b]. The overwhelming majority of the cases where unfavourable incremental segregation occurs can at least partly be attributed to repulsive interactions between solutes. Note that most unfavourable incremental segregation cases in the $\Sigma 3(1\bar{1}2)$ feature negligible solute interactions. In this case, the unfavourable incremental segregation of a second solute may be attributed to a lack of available strongly binding GB sites, and not the interactions themselves. This may be contrasted with the behaviour in the $\Sigma 9(2\bar{2}1)$ and $\Sigma 11(3\bar{3}2)$ GBs, where the role of significant repulsive interactions in deterring segregation in the unfavourable incremental segregation cases is apparent. Note the absolute majority of interactions even in the co-segregating cases tend to be negligible or repulsive, which informs us that co-segregation is mostly occurring in spite of, not due to, the co-segregation interactions. In the co-segregating cases, significant repulsive interactions dominate the interaction makeup of the $\Sigma 9(2\bar{2}1)$ and $\Sigma 11(3\bar{3}2)$, whereas negligible and attractive interactions dominate in the $\Sigma 3(1\bar{1}1)$. This supports our earlier observations about how local atomic structure significantly affects interactions, explaining why certain structures are intrinsically more favourable for co-segregation.

Single solute segregation may be energetically preferred to co-segregation in specific elemental combinations. Beyond cases where co-segregation is unfavourable ($E_{\text{seg}}^{\text{inc}} = 0$ eV), it is also possible for the X-Y to be co-segregating but energetically less favourable than a single solute segregated at the GB with the second solute situated in the bulk. There exist 45 heterogeneous X-Y elemental combinations for each GB, totalling 180 combinations that can be considered in this study. There are 33 cases that favour single-element segregation over co-segregation [grey in Table 5], resulting in 147 combinations where co-segregation is energetically favourable. There are 40 same-element (X-X) co-segregation cases, where 6 cases favour single-atom segregation, resulting in 34 favourable co-segregation cases. Combinations that yield a single-solute preference involve either weakly segregating (V/Cr/Co) or large elements (Nb/Mo/W), as noted prior.

3.5. Co-segregation and cohesion

Similar to the single solute study, we considered the cohesion effects of the co-segregated solutes. We quantified the cohesion effects at the minimum energy configuration at all considered cases in the Rice-Thomson-Wang framework. However, only the effects in the relaxed separation scheme at the most energetically favourable *combination* at each heterogeneous element-pairing are presented here in Table 5. For each solute-solute combination, the relaxed change in cohesion η and the corresponding total energy of segregation, $E_{\text{seg}}^{\text{tot}}$, are presented in Table 5 [Full data on both ordered elemental cases available in Supplementary Tables S41, S43]. Here, we do not include the combinations that are less energetically favourable than having one solute in the bulk and the other segregated, which are greyed out in Table 5. Most combinations of solutes studied here are cohesion enhancing, which is indicative of the effects of the single-segregated solutes generally transferring well to the pair-combinations, since most are cohesion enhancing individually. In particular, Nb, Mo and W are especially potent cohesion enhancers when segregated. On the other hand, note that the particularly potent embrittling effect of Cu in the $\Sigma 3(1\bar{1}2)$ tends to be reflected in all combinations. Particularly interesting is the behaviour of Ni, where its mixed role in cohesion is clear.

3.5.1. Co-segregation and cohesion: Configurational variations

Since the cohesion at each ordered pair configuration at all elemental combinations is known (i.e. X-Y vs Y-X segregation order-

Table 5

The effects of co-segregated solutes on GB cohesion (η) (lower left), and the total energy of segregation (upper right), are tabulated at the most energetically favourable configuration at each elemental combination. Same-element combinations are presented on the right, with the left column containing the cohesion effects and the right for total energy of segregation. The green, positive values indicate a cohesion enhancement effect, whereas cells shaded red indicate a decohesion effect. The more favourable segregation combinations, i.e. more negative values of total energy of segregation, are shaded in deeper blue. The 39 cells containing greyed-out values indicate that the single-element segregation displayed is energetically preferred over the combination. The element-wise distribution for the atoms that are purged from the combinations in these cases are (3V, 5Cr, 1Co, 1Mo, 1W), (6V, 5Cr, 4Co, 2W) and (5V, 3Cr, Mo, 2W), for the $\Sigma 3(112)$, $\Sigma 9(221)$ and $\Sigma 11(3\bar{3}2)$ GBs, respectively. The reader should refer to the Tables S16/S17 for the single-element values. The values in the cells correspond to the values found in the $\Sigma 3(1\bar{1}1)$, $\Sigma 3(1\bar{1}2)$, $\Sigma 9(2\bar{1}1)$ and $\Sigma 11(3\bar{3}2)$ GBs respectively. Copyable version in Supplementary Table S40.

Total E _{seg} (eV)										X-X Combos		
Ti	V	Cr	Mn	Co	Ni	Cu	Nb	Mo	W	Ti	V	
Ti	-0.59	-0.65	-0.96	-0.63	-0.87	-0.95	-1.40	-1.05	-0.98	0.09	-1.01	
	-0.11	Ti	-0.23	-0.11	-0.26	-0.33	-0.24	-0.15	-0.14	0.02	-0.15	
	Ti	-0.79	-1.09	-0.83	-1.07	-1.18	-1.03	-0.77	Ti	0.35	-0.83	
	-0.66	-0.65	-0.74	-0.75	-1.14	-1.18	-0.98	-0.75	-0.67	0.29	-0.74	
V	0.17		-0.24	-0.57	-0.27	-0.50	-0.60	-0.94	-0.58	-0.51	0.31	-0.18
	-0.03		Cr	Mn	-0.06	Ni	-0.24	Nb	Mo	W	N/A	N/A
	Ti	-0.22	Mn	-0.22	-0.50	-0.72	Nb	Mo	W	0.28	-0.12	
	0.38		Cr	Mn	-0.30	-0.65	-0.78	-0.93	-0.56	-0.51	0.37	-0.24
Cr	0.15	0.26		-0.63	-0.31	-0.58	-0.67	-0.97	-0.61	-0.55	0.28	-0.32
	Ti	Cr		-0.28	Cr	-0.19	-0.30	Nb	Mo	W	N/A	N/A
	0.41	0.33		Mn	-0.31	-0.64	-0.83	Nb	-0.47	-0.37	N/A	N/A
	0.41	Cr		Mn	-0.36	-0.63	-0.78	Nb	Mo	W	N/A	N/A
Mn	0.22	0.26	0.21		-0.63	-0.98	-1.06	-1.29	-0.94	-0.89	0.41	-0.94
	0.20	Mn	0.06		-0.20	-0.41	-0.52	-0.22	-0.28	-0.24	0.44	-0.47
	0.45	Mn	Mn		-0.62	-0.93	-1.10	-1.30	-0.76	-0.62	0.44	-0.88
	0.48	Mn	Mn		Mn	-0.85	-1.06	-1.02	-0.85	-0.75	0.58	-0.89
Co	0.01	0.18	0.01	0.12		-0.59	-0.71	-0.89	-0.52	-0.47	-0.04	-0.36
	-0.09	0.02	Cr	0.16		-0.17	-0.30	Nb	Mo	W	0.03	-0.07
	0.43	0.32	0.31	0.37		-0.58	-0.80	-1.07	-0.48	-0.35	0.16	-0.23
	0.50	0.47	0.44	Mn		-0.69	-0.83	-0.99	-0.57	-0.54	0.35	-0.32
Ni	-0.02	0.06	0.04	0.08	-0.06		-1.14	-1.13	-0.75	-0.67	-0.09	-0.82
	-0.27	Ni	-0.17	-0.20	-0.23		-0.54	-0.28	-0.16	Ni	-0.44	-0.38
	0.35	0.25	0.26	0.31	0.17		-1.11	-1.31	-0.73	-0.61	0.11	-0.88
	0.43	0.43	0.34	0.32	0.21		-1.09	-1.32	-0.88	-0.83	0.20	-0.94
Cu	-0.27	-0.12	-0.21	-0.02	-0.20	-0.18		-1.22	-0.89	-0.85	-0.41	-1.25
	-0.52	-0.46	-0.37	-0.46	-0.44	-0.60		-0.41	-0.31	-0.27	-0.81	-0.76
	-0.03	0.00	0.05	0.28	-0.07	-0.12		-1.39	-0.80	-0.67	-0.41	-1.26
	0.04	-0.15	0.00	0.05	-0.19	-0.15		-1.32	-0.92	-0.82	-0.41	-1.38
Nb	0.29	0.38	0.37	0.36	0.19	0.11	-0.14		-1.42	-1.34	0.51	-1.81
	0.06	Nb	Nb	-0.09	Nb	-0.30	-0.49		-0.17	-0.17	0.08	-0.32
	0.44	Nb	Nb	0.54	0.59	0.51	0.07		Nb	Nb	0.44	-1.04
	0.58	0.58	Nb	0.45	0.72	0.59	0.20		-0.92	-0.92	0.47	-1.03
Mo	0.42	0.54	0.52	0.47	0.35	0.23	0.12	0.66		-0.94	0.81	-1.02
	0.11	Mo	Mo	0.29	Mo	-0.04	-0.28	0.09		Mo	N/A	N/A
	0.60	Mo	0.51	0.49	0.56	0.47	0.02	Nb		-0.46	0.74	-0.53
	0.68	0.68	Mo	0.68	0.66	0.71	0.30	0.61		-0.65	1.05	-0.72
W	0.63	0.74	0.74	0.70	0.57	0.44	0.36	0.86	1.68		1.74	-0.86
	0.18	W	W	0.43	W	Ni	-0.42	0.13	Mo		N/A	N/A
	Ti	W	0.41	0.50	0.39	0.63	-0.09	Nb	0.88		0.94	-0.32
	0.85	0.65	W	0.64	0.70	0.79	0.11	0.61	1.39		1.38	-0.57
η (J/m ²)												

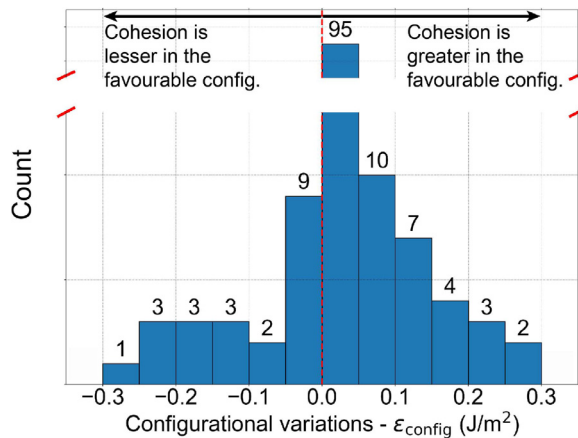


Fig. 4. A histogram depiction of the distribution of differences in cohesive effect that arise due to configurational variations that occur across all heterogeneous X-Y co-segregating elemental combinations. This is calculated by taking the difference in cohesive effect at the energetically favourable configuration and its less favourable counterpart at each combination i.e. $\epsilon_{\text{config}} = \eta[\min_E(X+Y, Y+X)] - \eta[\max_E(X+Y, Y+X)]$. There are 142 (45, 25, 34, 38) computed values in total, available in Supplementary Table S50.

ing), it is possible to compute the difference in the cohesion effects at each configuration in each combination. We termed this difference “configurational variation” (ϵ_{config}). The distribution of the ϵ_{config} values that arise as a result of this comparison is presented in Fig. 4. We did not compute ϵ_{config} for cases where $E_{\text{seg}}^{\text{inc}} = 0$ eV or unavailable (V-X in $\Sigma 3(1\bar{1}2)$) in either ordered pair, for a specific elemental combination. Simply, this allows the determination of whether cohesion effects vary as a function of solute segregation position and sequence at the GB. A positive value of ϵ_{config} indicates that the favourable configuration has a higher cohesion than the less favourable configuration, whereas negative values indicate the opposite. The data is available in full in Supplementary Table S50.

From Fig. 4, we may conclude that the cohesion effects of co-segregated pairs may be computed accurately in most cases without consideration of configurational arrangement (i.e. segregation order). The number of errors that are larger than 0.1 J/m² number 26 (5, 7, 9, 5). The proportion of cases where $|\epsilon_{\text{config}}| < 0.05$ J/m² is 74%, and 83% where $|\epsilon_{\text{config}}| < 0.1$ J/m². However, note that cases which differ by less than 0.01 eV in the total energy at the same elemental combination can have significantly different effects on GB cohesion. For example, the Ni-W and W-Ni ordered pair configurations in the $\Sigma 9(\bar{2}\bar{1})$ GB differ only by 0.005 eV in total energy, but the cohesive effect in the favoured configuration is +0.63 J/m², and only +0.40 J/m² in the less favoured configuration [Supplementary Tables S43, S49]. Furthermore, the calculated ϵ_{config} values range $-0.08 < \epsilon_{\text{config}} < 0.17$, $-0.23 < \epsilon_{\text{config}} < 0.28$, $-0.27 < \epsilon_{\text{config}} < 0.23$, $-0.20 < \epsilon_{\text{config}} < 0.21$ J/m² for the $\Sigma 3(1\bar{1}1)$, $\Sigma 3(1\bar{1}2)$, $\Sigma 9(2\bar{2}1)$, $\Sigma 11(3\bar{3}2)$ GBs, respectively. Therefore, the cohesion effects enacted by co-segregated solutes can be substantially altered by their positional configuration at a GB.

3.5.2. Co-segregation and cohesion: Linear approximations vs actual effects

The importance of co-segregation on GB cohesion may be examined by a comparison of the cohesion effect of a co-segregated pair of atoms with their summed single solute cohesion effects. This is essentially a comparison of a linear approximation to the combined effect. We term the difference between these two

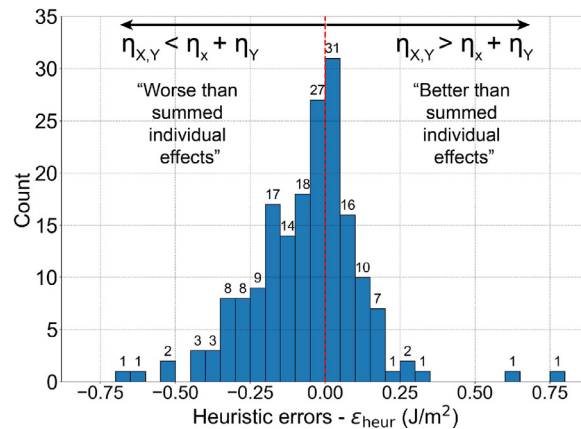


Fig. 5. A histogram depiction of the distribution of heuristic errors in each elemental combination that arise by estimating the cohesive effect of a co-segregating combination by summing the individual effects of each solute, i.e. $\epsilon_{\text{heur}} = \eta_{X,Y} - (\eta_X + \eta_Y)$. A total of 181 (55, 35, 44, 47) values were computed [see text], available in full in Supplementary Table S47. Positive values indicate that the cohesion effect derived of the summed individual effects is lesser than the true computed effect on cohesion (i.e. GB cohesion is better than expected), whereas negative values indicate the opposite.

quantities the heuristic error, ϵ_{heur} . We exclude the cases where co-segregation is unfavourable, resulting in a total of 181 computed values out of 220 possible pair combinations (180 heterogeneous + 40 same-element pairings). The distribution of the ϵ_{heur} values are presented in Fig. 5 and Table S47. The heuristic errors range $-0.12 < \epsilon_{\text{heur}} < 0.79$, $-0.35 < \epsilon_{\text{heur}} < 0.18$, $-0.44 < \epsilon_{\text{heur}} < 0.34$, $-0.67 < \epsilon_{\text{heur}} < 0.26$ J/m² for the $\Sigma 3(1\bar{1}1)$, $\Sigma 3(1\bar{1}2)$, $\Sigma 9(2\bar{2}1)$, $\Sigma 11(3\bar{3}2)$ GBs respectively. The number of cases where $|\epsilon_{\text{heur}}| > 0.1$ J/m² is 88 (13, 20, 19, 36), which is 49% of the total. We calculated the relative size of these heuristic errors to the magnitude of the calculated combined effect, revealing that the size of ϵ_{heur} can be up to 274% the magnitude of the actual cohesive effect.

3.6. A link between chemical bonding and work of separation

Finally, GB cohesion is intrinsically related to the strength of the interfacial atomic bonding present. To investigate this relationship, we calculated the strength of the bonds, as measured by bond orders in the DDEC6 framework [35], that pass through the cleavage plane and compared it to the work required to separate the interface at that plane. We plot this comparison across the weakest cleavage planes at the interface [Fig. 6], as measured by $W_{\text{sep}}^{\text{RGS}}$, across all the single solute segregation and co-segregated pairings considered in this study. Comparisons are plotted against the calculated W_{sep} values in both rigid and relaxed frameworks, for Figs. 6a and 6b, respectively. There exists a strong positive correlation between the two quantities, which is evidenced by the Pearson correlation coefficients (R) calculated for each GB, ranging 0.781-0.893 and 0.730-0.911 respectively for the two cases in Fig. 6. The overall correlation coefficients for the two datasets are 0.801 and 0.760, respectively. This relationship functions regardless of whether surface relaxations are included or not (i.e. rigid vs relaxed) in the W_{sep} calculations. However, the agreement is generally better with the W_{sep} quantities calculated in the rigid calculation framework (i.e. $W_{\text{sep}}^{\text{RGS}}$ in Fig. 6a). This is rationalised by the fact that the energy required to break bonds is better represented by the difference in energy states between the GB and a freshly fractured non-equilibrium surface state, compared to the final energy-state of a relaxed surface. An additional comparison

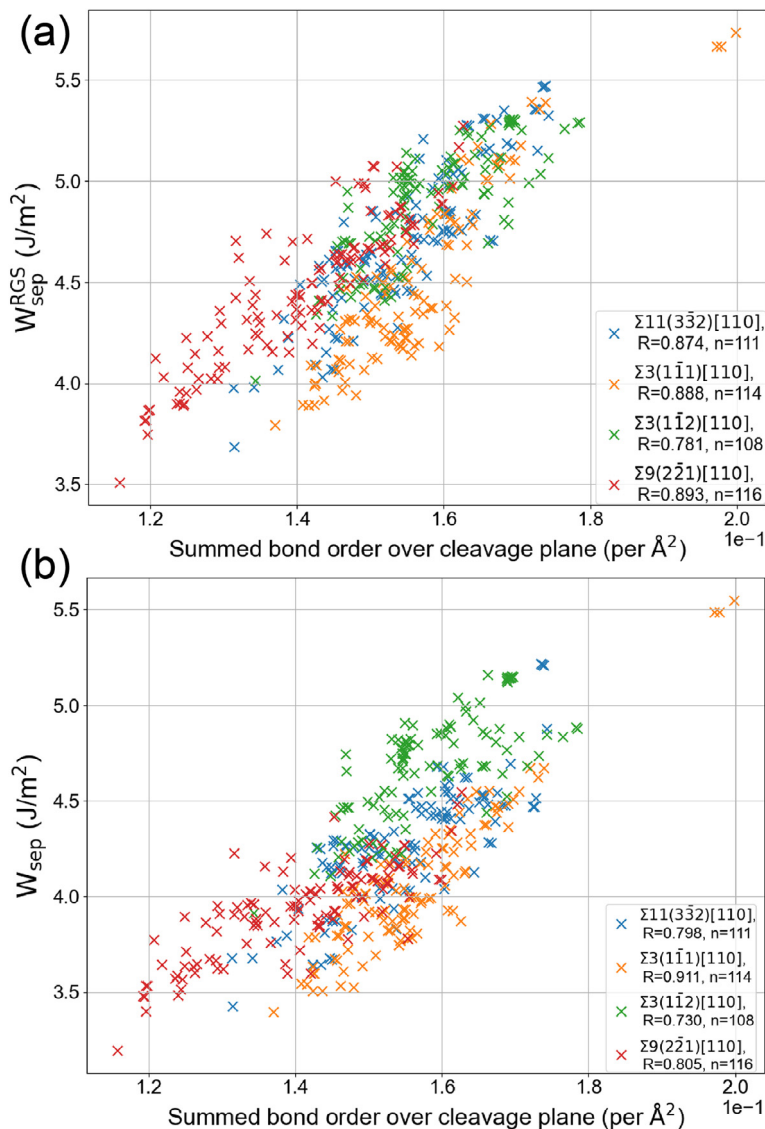


Fig. 6. The works of separation in both the rigid and relaxed separation frameworks (Methods) are plotted against the summed strength of the bond-orders passing through the cleavage plane. (6a) The minimum (i.e. at the weakest plane of separation) W_{sep}^{RGS} (*rigid*) in all studied cases are plotted. (6b) The corresponding W_{sep} (*relaxed*) is plotted. R is the correlation (Pearson) coefficient calculated for the GB datasets, and n the number of cases that were considered for each GB. The bond-order data is available in Supplementary Tables S51-S55.

plot of the results involving all studied cleavage planes is provided in Supplementary Fig. S68.

4. Discussion

Our calculations reveal that the segregation behaviours of transition metals in α -Fe are dependent on GB character. Notably, stacking-fault/twin type GBs (represented by the $\Sigma 3(1\bar{1}\bar{2})$), which are characterised by their high coherency, significantly lower excess volumes and GB energies, are weak trappers of solutes compared to other archetypes. Additionally, this GB has a higher cohesive strength compared to its peers. While drastic differences in GB character, as quantified by excess volumes and GB energies, can strongly predict the favourability of a GB for segregation, small differences in these characteristic quantities cannot be used to predict such matters. Instead, it depends on the specific site environments available in the GB, i.e. the local atomic structure present. This is evidenced by the differing energetic preferencing rankings

of elemental (single-solute) segregation to the GBs. We find that site volume, quantified on a Voronoi volume basis, is an important factor in determining elemental segregation favourability at different sites in the GB. Large solutes tend to prefer sites with larger Voronoi volumes, in both single and co-segregation cases [see S.I., Figs. S6-S15, S38-S47]. This has important implications for site-competition phenomena and GB engineering. The cohesion effects of even the same segregated element can vary drastically between different GBs.

Our study demonstrates that segregation in Fe-based alloys is not solely determined by the solutes and GBs, but also the interactions occurring between pairs of sequentially segregating solutes. Beyond specific extraordinary attractive co-segregation interactions, which are demonstrably rare between transition metals in this study, the majority tend to be overwhelmingly mild or repulsive in nature. This is similar to that in the bulk [28] or for GBs for selected solutes in Fe [16,23,26,27]. Elements which exhibit weak segregation to the pure GB often may not segregate to prior-

decorated GBs, due to the repulsive interactions with the prior-segregated atoms. GB character plays an important role in these interactions - the aforementioned effect is especially pronounced in GBs where few sites are favourable for segregation and/or have weak segregation binding at those sites. On the other hand, GBs which possess a large amount of such favourable sites per unit interface area in the single-solute case does not necessarily guarantee that it is favourable for significant amounts of co-segregation. An example of this lies in the variance of the computed interactions between large solutes, ranging from significantly repulsive to attractive in varying GB characters, which can encourage or discourage further co-segregation of large solutes at different GBs. Finally, these interactions can vary widely in their nature and magnitude, as a function of their position, element, and GB character, a point of discussion in the following. These facts reinforce the importance of an explicit case-by-case consideration of a range of GB archetypes when studying the effects of solute interactions and segregation on GB cohesion.

Although there is qualitative agreement between the interactions that occur between solutes in the bulk and at GBs, the solute-solute interactions in the bulk are generally a poor proxy for modelling interactions at the GB. The interactions that may occur between co-segregating transition metals are diverse, wide-ranging in both character and magnitude, varying as a function of GB structure. Such interactions may be significantly repulsive, which may completely discourage further segregation, or attractive, encouraging more segregation at the GB, as demonstrated by Table 4. A quantitative, 1:1 comparison of bulk solute-solute interactions to those occurring at a GB is difficult to perform due to the nature of less well-defined distances that occur at the GB compared to the bulk. This necessitates some kind of interpolative spline curve-fitting, or taking the interaction at the closest distance between solutes (at the GB vs bulk). This is possible by comparison with the data provided by Gorbatov et al. in Ref. [28]. However, we prefer not to do this since the validity of comparing interactions quantitatively directly in either manner is questionable. Nevertheless, it is possible to qualitatively demonstrate why this is a poor assumption to make, using the range of interactions observed in the computed minimum energy configurations.

We demonstrate using examples of why solute-solute interactions in the bulk are a poor proxy for modelling them at the GB. Let us use the example of Cu-Cu in the bulk, where they attract each other with strength $-0.23 \text{ eV} \rightarrow -0.08 \text{ eV}$ in the 1st \rightarrow 3rd coordination shells [28]. This same Cu-Cu interaction can range $-0.60 \text{ eV} \rightarrow -0.13 \text{ eV}$ at the minimum energy configurations in the four GBs in this study. Another example includes that of the interactions that occur between large solutes (Nb, Ti, W, Mo). Their interactions can range from largely repulsive in the $\Sigma 9(2\bar{2}1)$ and $\Sigma 11(3\bar{3}2)$ GBs, attractive for the $\Sigma 3(1\bar{1}1)$ GB, and are negligible to repulsive in the $\Sigma 3(1\bar{1}2)$. For comparison, these solutes are exclusively significantly repulsive in the first and second coordination shells in the bulk, with values $0.11 \text{ eV} < E_{\text{int}} < 0.41 \text{ eV}$ [28]. In the GB, our calculated interactions at the minimum energy configurations range $-0.26 \text{ eV} < E_{\text{int}} < 0.79 \text{ eV}$. The local atomic structures play a critical role in determination of these interactions between large solutes - large repulsive interactions occur in GBs where additional sites with large Voronoi volumes are unavailable. The local structure of the $\Sigma 3(1\bar{1}1)$ GB renders it more suitable for accommodating multiple oversized solutes, a fact that is partially reflected in it possessing the largest excess volume of the GBs studied. So, for the example of large solutes, the variance in interaction behaviours would render an extrapolation from bulk interactions invalid.

Further examples include the interactions between the Ni-Cu (-0.59 eV) and Cu-Cu (-0.60 eV) pairings in the $\Sigma 3(1\bar{1}1)$ GB, which can result in extraordinary attraction behaviour resulting in segre-

gation binding at sites whose strength are over four times of the same site in the pure Fe GB ($E_{\text{seg}}^{\text{pure}} \text{ Cu in Ni-Cu: } -0.137 \text{ eV}$, $E_{\text{seg}}^{\text{pure}} \text{ Cu in Cu-Cu: } -0.137 \text{ eV}$). In the case where the order is reversed, in the Cu-Ni case, the interaction is only mildly attractive (-0.05 eV), indicating that the interaction is a function of the position of the segregated solutes. In this case, the Ni-Cu case becomes favoured over the Cu-Ni case due to the extraordinary interaction between solutes ($E_{\text{seg}}^{\text{inc}} \text{ Ni-Cu: } -1.14 \text{ eV}$, $E_{\text{seg}}^{\text{inc}} \text{ Cu-Ni: } -0.97 \text{ eV}$). This cannot be predicted on a single solute basis, which predicts Cu to bind more strongly to the GB (-0.509 eV vs -0.413 eV). On the other hand, the same Ni-Cu case in the $\Sigma 11(3\bar{3}2)$ GB has a repulsive interaction. The Ni-Cu interactions in the bulk are demonstrated to be only mildly attractive, with an E_{int} of -0.08 eV , -0.02 eV and 0.02 eV [28], compared to the computed values here of $-0.59 \text{ eV} \rightarrow 0.22 \text{ eV}$ for the different GBs. These examples demonstrate the importance of explicit and thorough treatment of co-segregation effects, and why bulk solute-solute interactions cannot be used as a proxy for GB co-segregation interactions. These interactions play a critical role in co-segregation, and can vary wildly as a function of GB character, position, and element. So, although there is relatively good overall qualitative agreement for the nature of solute-solute interactions at the bulk and GB, this is a dangerous quantitative extrapolation to make in modelling GB co-segregation, due to the nature of unique local GB atomic environments substantially altering interaction behaviours.

As a final note on co-segregation effects, we ask, exactly how important are they with respect to cohesion? The importance of co-segregation effects may be illustrated by comparing the combined effects of co-segregated solutes at the GB with their summed individual effects [Fig. 5]. The effects of co-segregated solutes on cohesion can be up to two times the size of their summed individual effects, even when only including significant effects (i.e. $\eta_{X,Y} > 0.1 \text{ J/m}^2$). We have also demonstrated that solute configurations that differ by less than 0.01 eV can have drastically different effects on GB cohesion - demonstrating that configurational arrangement also plays a critical role in cohesion (e.g. the Ni-W cases in the $\Sigma 9(2\bar{2}1)$ GB). Such configurational variations can result in variance in the cohesion effect in excess of twice the magnitude of the effect in the energetically favourable configuration. Thus, careful consideration of the positioning of co-segregated solutes is necessary when assessing their effects on GB cohesion. Recall that the energetic favourability of specific configurational arrangements depends heavily on the interactions that occur between solutes - which in turn, vary according to the local GB environment, elements involved and positions of the solutes. Therefore, co-segregation effects play a significant role in the cohesion of the GB interfaces.

We have demonstrated quantitatively that the chemical and physical aspects of interface cohesion are intimately linked. This is apparent in the strong positive correlation between the quantities of the strength of bonding (chemical) passing through a plane at any GB and the amount of work (physical) that is required to separate it at that plane. Importantly, this relationship appears to be generally applicable across different GBs, an observation that may be justified intuitively in that stronger bonds result in a higher W_{sep} of the interface [Fig. 6]. Chemical bond order analysis of interface cohesion is orders of magnitude cheaper in computational cost compared to work of separation calculations performed in the Rice-Thomson-Wang framework. Furthermore, some have argued that a more intuitive and accurate method of determination of interfacial cohesion is through the analysis of the strength of bonding [50,51]. However, a rigorous definition of bond-orders, a measure of bonding strength, was lacking until recently [35]. For the case of transition metals in α -Fe GBs, we have demonstrated that there is relatively good agreement between the commonly used W_{sep} quantity in Rice-Thomson-Wang theory and

the area-normalised summed bond-orders in the DDEC6 framework over the interfacial cleavage plane. Future studies of interfacial cohesion should additionally incorporate bonding-based analysis as introduced here. Our findings indicate that *rigid* separation methodologies of calculating W_{sep} (i.e. without relaxation of the surface) are a better representation of the energies required to cleave the bonds at the GB. Thus, *rigid* W_{sep} calculations should be a more accurate representation of the mechanics of intergranular fracture. Lastly, we note the considerable ranges of W_{sep} and summed bond orders which are observed across the four GBs in Figs 6a and 6b. This serves as a striking visual representation of the rich diversity of cohesion behaviours that can occur at GBs, depending on the segregated/co-segregated solutes present.

For the purposes of comparison of our results with experiments, we note that experimentally measured segregation energies at GBs are, by their nature, area-averaged values due to resolution limits of experimental techniques. Due to this, they observe an artificial temperature dependence in their derived segregation energies [52,53]. This is contrasted with generated results from first-principles calculations and other simulations, which may evaluate the full spectra of segregation energies at a GB on a per-site basis [52,54,55]. This fundamental difference in the calculated and measured quantities can result in a large disparity between experiment and simulation results when compared, as seen in Lejček's review [21]. According to a recent work [53], the nature of averaged segregation energies in experiments was the cause of this artificial temperature dependence compared to DFT generated predictions. Good agreement between DFT predictions of segregation coverage and experimentally measured results at ferritic Fe GBs was achieved when accounting for the spectral nature of segregation energies at an interface, without the consideration of other temperature effects (e.g. configurational entropy/phonons/finite temperature magnetic effects). As such, we expect such effects to be similarly negligible here for temperatures up to 0.5 of T_m (melting temperature) and small at up to 0.75 of T_m , as observed in their study.

Regarding finite temperature effects on energetics, the total free energy changes that result from phonons and magnetic effects have previously been investigated using a coupled formulation in bcc Fe [56]. Their combined effect on the total free energy was calculated to be less than 20 meV/atom in the temperature range 0–800 K. As such, the finite temperature effects of magnetism and phonons are effectively negligible on the energetics of segregation/co-segregation. Other factors, such as the selected calculation parameters, generate variance of a similar magnitude in the calculated total energies.

Lastly, solute-solute interactions, even those that occur in the bulk, are generally not accessible directly through experiments [28]. Currently, direct quantification of these interactions is exclusively the domain of simulations. Experimental measures of these interactions are generally indirectly inferred from results, such as generated phase diagrams or short-range order measurements. However, recent studies of bi-crystals and grain boundaries have allowed certain interactive co-segregation phenomena to be observed, where experimental results have shown good qualitative agreement with DFT predictions [26,57]. As such, we expect the results here to be a useful quantitative guide to transition metal-transition metal interactions and how they affect cohesion in iron GBs.

5. Conclusion

To conclude, we have utilised DFT calculations to provide a comprehensive evaluation of the segregation, co-segregation and cohesion effects of common alloying transition metals to vary-

ing α -Fe GBs. We revealed that the segregation behaviours and resultant cohesion effects of transition metals cannot be generalised on a purely elemental basis, since they vary as a function of GB character. The effects of co-segregated solutes on GB cohesion can vary drastically from their summed individual elemental effects. The interactions occurring between solutes at GBs can control co-segregation, and are a function of solute positioning, element and the local GB interface structure. These solute-solute interactions at GBs are demonstrated to diverge significantly from those observed in bulk α -Fe. The differing local atomic structures present at GBs can cause these interactions to vary drastically, even amongst GBs with similar GB energies and excess volumes. Finally, we have demonstrated a quantitative method of calculating interfacial cohesion at a GB through assessing the strength of bonds present, by introducing the area-normalised summed bond order quantity. There is general agreement between this bonding-based quantity and the works of separation calculated in the Rice-Thomson-Wang framework for the case of segregated transition metals in α -Fe GBs. Combined, these insights will be valuable in enabling rational GB engineering of steels through transition metal alloying.

Data availability

Data is available from the corresponding author upon reasonable request. We kindly ask readers to carefully peruse the Supplementary Information before making such a request, as extensive datasets/structure files etc. are available in there.

Author contributions

H.L. Mai conceived parts of the methodology (bond-order analysis), implemented the methodology, setup and performed the DFT calculations, performed the post-processing and data analysis, and prepared the initial draft of the manuscript. X.Y. Cui supported technical analysis required for certain calculations, provided calculation resource management, and provided co-supervision. D. Scheiber and L. Romaner contributed to formulation of the methodological implementation. S. Ringer conceived and supervised the work, and leads the ongoing project for which this work is part of. All authors contributed to the manuscript.

Declaration of Competing Interest

The authors declare that there are no competing interests.

Acknowledgements

H.L. Mai gratefully acknowledges the research-enabling financial support provided by the University of Sydney and the Australian Government, via the Top-up and Research Training Program (RTP) scholarships, respectively. We acknowledge support from the [Australian Research Council \(DP160101713, LP190101169\)](#) and the Australia-US Multidisciplinary University Research Initiative (AUS-MURI) program supported by the Australian Government via the Department of Defence under the Next Generation Technologies Fund. The authors acknowledge the facilities and both the scientific and technical assistance of staff from Sydney Microscopy and Microanalysis, which is the University of Sydney node of Microscopy Australia. This work was supported by computational resources provided by the Australian Government through the National Computational Infrastructure (Gadi) and the Pawsey Supercomputing Centre (Magnus) under the National Computational Merit Allocation Scheme. Additional resource support facilitated by the team at the Sydney Informatics Hub (the University of Sydney)

is gratefully acknowledged (LE190100021). Both Microscopy Australia and the NCI are supported by the Australian Government's National Collaborative Research Infrastructure Scheme (NCRIS). L. Romaner acknowledges funding by the Austrian Science Fund (FWF) [P 34179].

Supplementary material

Supplementary material associated with this article can be found, in the online version, at doi:[10.1016/j.actamat.2022.117902](https://doi.org/10.1016/j.actamat.2022.117902).

References

- [1] T. Watanabe, An approach to grain boundary design for strong and ductile polycrystals, *Res mechanica* 11 (1) (1984) 47–84.
- [2] P. Lejček, *Grain boundary segregation in metals*, volume 136, Springer Science & Business Media, 2010.
- [3] M.A. Gibson, C.A. Schuh, A compilation of ab-initio calculations of embrittling potencies in binary metallic alloys, *Data Brief* 6 (2016) 143–148, doi:[10.1016/j.dib.2015.11.024](https://doi.org/10.1016/j.dib.2015.11.024).
- [4] S. Bechtel, M. Kumar, B.P. Somerday, M.E. Launey, R.O. Ritchie, Grain-boundary engineering markedly reduces susceptibility to intergranular hydrogen embrittlement in metallic materials, *Acta Mater* 57 (14) (2009) 4148–4157.
- [5] X. Zhou, X.-x. Yu, T. Kaub, R.L. Martens, G.B. Thompson, Grain boundary specific segregation in nanocrystalline Fe (Cr), *Sci Rep* 6 (1) (2016) 1–14.
- [6] K.A. Darling, B.K. VanLeeuwen, J.E. Semones, C.C. Koch, R.O. Scattergood, L.J. Kecskes, S.N. Mathaudhu, Stabilized nanocrystalline iron-based alloys: guiding efforts in alloy selection, *Materials Science and Engineering: A* 528 (13) (2011) 4365–4371, doi:[10.1016/j.msea.2011.02.080](https://doi.org/10.1016/j.msea.2011.02.080).
- [7] Y. Li, D. Raabe, M. Herbig, P.-P. Choi, S. Goto, A. Kostka, H. Yarita, C. Borchers, R. Kirchheim, Segregation stabilizes nanocrystalline bulk steel with near theoretical strength, *Phys. Rev. Lett.* 113 (10) (2014) 106104, doi:[10.1103/PhysRevLett.113.106104](https://doi.org/10.1103/PhysRevLett.113.106104).
- [8] I. Olefjord, Temper embrittlement, *International Metals Reviews* 23 (1) (1978) 149–163, doi:[10.1179/imtr.1978.23.1.149](https://doi.org/10.1179/imtr.1978.23.1.149).
- [9] S. Lynch, Hydrogen embrittlement phenomena and mechanisms, *Corros. Rev.* 30 (3–4) (2012) 105–123, doi:[10.1515/correv-2012-0502](https://doi.org/10.1515/correv-2012-0502).
- [10] T. Meiners, T. Frolov, R.E. Rudd, G. Dehm, C.H. Liebscher, Observations of grain-boundary phase transformations in an elemental metal, *Nature* 579 (7799) (2020) 375–378, doi:[10.1038/s41586-020-2082-6](https://doi.org/10.1038/s41586-020-2082-6).
- [11] A.C. Day, A.V. Ceguerra, S.P. Ringer, Introducing a crystallography-mediated reconstruction (CMR) approach to atom probe tomography, *Microsc. Microanal.* 25 (2) (2019) 288–300, doi:[10.1017/S1431927618015593](https://doi.org/10.1017/S1431927618015593).
- [12] A. P. A. Subramanyam, A. Azócar Guzmán, S. Vincent, A. Hartmaier, R. Janisch, Ab initio study of the combined effects of alloying elements and h on grain boundary cohesion in ferritic steels, *Metals (Basel)* 9 (3) (2019) 291, doi:[10.3390/met9030291](https://doi.org/10.3390/met9030291).
- [13] W.T. Geng, A.J. Freeman, G.B. Olson, Influence of alloying additions on grain boundary cohesion of transition metals: first-principles determination and its phenomenological extension, *Physical Review B* 63 (16) (2001) 165415, doi:[10.1103/PhysRevB.63.165415](https://doi.org/10.1103/PhysRevB.63.165415).
- [14] L. Zhong, R. Wu, A.J. Freeman, G.B. Olson, Effects of Mn additions on the Pembrittlement of the fe grain boundary, *Physical Review B* 55 (17) (1997) 11133–11137, doi:[10.1103/PhysRevB.55.11133](https://doi.org/10.1103/PhysRevB.55.11133).
- [15] K. Ito, H. Sawada, S. Ogata, First-principles study on the grain boundary embrittlement of bcc-fe by mn segregation, *Physical Review Materials* 3 (1) (2019) 013609, doi:[10.1103/PhysRevMaterials.3.013609](https://doi.org/10.1103/PhysRevMaterials.3.013609).
- [16] H. Jin, I. Elfimov, M. Militzer, Study of the interaction of solutes with Σ5 (013) tilt grain boundaries in iron using density-functional theory, *J Appl Phys* 115 (9) (2014) 093506, doi:[10.1063/1.4867400](https://doi.org/10.1063/1.4867400).
- [17] M. Yamaguchi, J. Kameda, Multiscale thermodynamic analysis on fracture toughness loss induced by solute segregation in steel, *Philos. Mag.* 94 (19) (2014) 2131–2149, doi:[10.1080/14786435.2014.906757](https://doi.org/10.1080/14786435.2014.906757).
- [18] Y.-J. Hu, Y. Wang, W.Y. Wang, K.A. Darling, L.J. Kecskes, Z.-K. Liu, Solute effects on the Σ3 11[11-0] tilt grain boundary in BCC Fe: grain boundary segregation, stability, and embrittlement, *Comput. Mater. Sci.* 171 (2020) 109271, doi:[10.1016/j.commatsci.2019.109271](https://doi.org/10.1016/j.commatsci.2019.109271).
- [19] E. Wachowicz, T. Ossowski, A. Kiejna, Cohesive and magnetic properties of grain boundaries in bcc Fe with Cr additions, *Physical Review B* 81 (9) (2010) 094104, doi:[10.1103/PhysRevB.81.094104](https://doi.org/10.1103/PhysRevB.81.094104).
- [20] Z.-Z. Chen, C.-Y. Wang, First-principles study on the effects of co-segregation of Ti, b and o on the cohesion of the α-fe grain boundary, *J. Phys.: Condens. Matter* 17 (42) (2005) 6645–6652, doi:[10.1088/0953-8984/17/42/005](https://doi.org/10.1088/0953-8984/17/42/005).
- [21] P. Lejček, M. Sób, V. Paidar, Interfacial segregation and grain boundary embrittlement: an overview and critical assessment of experimental data and calculated results, *Prog Mater Sci* 87 (2017) 83–139, doi:[10.1016/j.pmatsci.2016.11.001](https://doi.org/10.1016/j.pmatsci.2016.11.001).
- [22] Z. Xu, S. Tanaka, M. Kohyama, Grain-boundary segregation of 3d-transition metal solutes in bcc fe: ab initio local-energy and d-electron behavior analysis, *J. Phys.: Condens. Matter* 31 (11) (2019) 115001, doi:[10.1088/1361-648X/aa1d00](https://doi.org/10.1088/1361-648X/aa1d00).
- [23] A.S. Kholtobina, W. Ecker, R. Pippan, V.I. Razumovskiy, Effect of alloying elements on hydrogen enhanced decohesion in bcc iron, *Comput. Mater. Sci.* 188 (2021) 110215, doi:[10.1016/j.commatsci.2020.110215](https://doi.org/10.1016/j.commatsci.2020.110215).
- [24] T. Schuler, F. Christien, P. Ganster, K. Wolski, Ab initio investigation of phosphorus and hydrogen co-segregation and embrittlement in α-fe twin boundaries, *Appl Surf Sci* 492 (2019) 919–935, doi:[10.1016/j.apsusc.2019.04.025](https://doi.org/10.1016/j.apsusc.2019.04.025).
- [25] B. He, W. Xiao, W. Hao, Z. Tian, First-principles investigation into the effect of Cr on the segregation of multi-H at the fe Σ3 (111) grain boundary, *J. Nucl. Mater.* 441 (1) (2013) 301–305, doi:[10.1016/j.jnucmat.2013.06.015](https://doi.org/10.1016/j.jnucmat.2013.06.015).
- [26] A. Ahmadian, D. Scheiber, X. Zhou, B. Gault, C.H. Liebscher, L. Romaner, G. Dehm, Aluminum depletion induced by complex co-segregation of carbon and boron in a Σ5 [3 1 0] bcc-iron grain boundary, *Nat Commun* (2021).
- [27] D. Scheiber, K. Prabitz, L. Romaner, W. Ecker, The influence of alloying on Zn liquid metal embrittlement in steels, *Acta Mater* 195 (2020) 750–760, doi:[10.1016/j.actamat.2020.06.001](https://doi.org/10.1016/j.actamat.2020.06.001).
- [28] O. Gorbatov, A. Hosseiniزاده Delandar, Y. Gornostyrev, A. Ruban, P. Korzhavyi, First-principles study of interactions between substitutional solutes in bcc iron, *J. Nucl. Mater.* 475 (2016) 140–148, doi:[10.1016/j.jnucmat.2016.04.013](https://doi.org/10.1016/j.jnucmat.2016.04.013).
- [29] D. Scheiber, L. Romaner, R. Pippan, P. Puschnig, Impact of solute-solute interactions on grain boundary segregation and cohesion in molybdenum, *Physical Review Materials* 2 (9) (2018) 093609, doi:[10.1103/PhysRevMaterials.2.093609](https://doi.org/10.1103/PhysRevMaterials.2.093609).
- [30] S.K. Bhattacharya, S. Tanaka, Y. Shiihara, M. Kohyama, Ab initio perspective of the (110) symmetrical tilt grain boundaries in bcc Fe: application of local energy and local stress, *J Mater Sci* 49 (11) (2014) 3980–3995, doi:[10.1007/s10853-014-8038-1](https://doi.org/10.1007/s10853-014-8038-1).
- [31] H. Nakashima, M. Takeuchi, Grain boundary energy and structure of α-Fe<110> symmetric tilt boundary, *Tetsu-to-Hagané* 86 (5) (2000) 357–362, doi:[10.2355/tetsutohagané1955.86.5_357](https://doi.org/10.2355/tetsutohagané1955.86.5_357).
- [32] S.K. Bhattacharya, S. Tanaka, Y. Shiihara, M. Kohyama, Ab initio study of symmetrical tilt grain boundaries in bcc Fe: structural units, magnetic moments, interfacial bonding, local energy and local stress, *J. Phys.: Condens. Matter* 25 (13) (2013) 135004, doi:[10.1088/0953-8984/25/13/135004](https://doi.org/10.1088/0953-8984/25/13/135004).
- [33] J.R. Rice, R. Thomson, Ductile versus brittle behaviour of crystals, *The Philosophical Magazine: A Journal of Theoretical Experimental and Applied Physics* 29 (1) (1974) 73–97.
- [34] J.R. Rice, J.-S. Wang, Embrittlement of interfaces by solute segregation, *Materials Science and Engineering: A* 107 (1989) 23–40.
- [35] T. A. Manz, Introducing DDEC6 atomic population analysis: Part 3. comprehensive method to compute bond orders, *RSC Adv* 7 (72) (2017) 45552–45581, doi:[10.1039/C7RA07400J](https://doi.org/10.1039/C7RA07400J).
- [36] P.E. Blöchl, Projector augmented-wave method, *Physical Review B* 50 (24) (1994) 17953.
- [37] G. Kresse, J. Hafner, Ab initio molecular dynamics for liquid metals, *Physical Review B* 47 (1) (1993) 558.
- [38] G. Kresse, J. Furthmüller, Efficient iterative schemes for ab initio total-energy calculations using a plane-wave basis set, *Physical Review B* 54 (16) (1996) 11169–11186, doi:[10.1103/PhysRevB.54.11169](https://doi.org/10.1103/PhysRevB.54.11169).
- [39] J.P. Perdew, K. Burke, M. Ernzerhof, Generalized gradient approximation made simple, *Phys. Rev. Lett.* 77 (18) (1996) 3865–3868, doi:[10.1103/PhysRevLett.77.3865](https://doi.org/10.1103/PhysRevLett.77.3865).
- [40] A.H. Larsen, J.J. Mortensen, J. Blomqvist, I.E. Castelli, R. Christensen, M. Dušlák, J. Friis, M.N. Groves, B. Hammer, C. Hargus, The atomic simulation environment—a Python library for working with atoms, *J. Phys.: Condens. Matter* 29 (27) (2017) 273002.
- [41] A.P. Sutton, *Interfaces in crystalline materials*, Monographs on the Physics and Chemistry of Materials (1995) 414–423.
- [42] A. Pineau, A.A. Benzerga, T. Pardo, Failure of metals I: brittle and ductile fracture, *Acta Mater* 107 (2016) 424–483, doi:[10.1016/j.actamat.2015.12.034](https://doi.org/10.1016/j.actamat.2015.12.034).
- [43] V.I. Razumovskiy, A.Y. Lozovoi, I.M. Razumovskii, First-principles-aided design of a new Ni-base superalloy: influence of transition metal alloying elements on grain boundary and bulk cohesion, *Acta Mater* 82 (2015) 369–377, doi:[10.1016/j.actamat.2014.08.047](https://doi.org/10.1016/j.actamat.2014.08.047).
- [44] D. McLean, A. Maradudin, Grain boundaries in metals, *Phys Today* 11 (1958) 35, doi:[10.1063/1.3062658](https://doi.org/10.1063/1.3062658).
- [45] C.L. White, W.A. Coglan, The spectrum of binding energies approach to grain boundary segregation, *Mettal. Trans. A* 8 (9) (1977) 1403–1412.
- [46] D.L. Olmsted, S.M. Foiles, E.A. Holm, Survey of computed grain boundary properties in face-centered cubic metals: I. Grain boundary energy, *Acta Mater* 57 (13) (2009) 3694–3703, doi:[10.1016/j.actamat.2009.04.007](https://doi.org/10.1016/j.actamat.2009.04.007).
- [47] M. Militzer, J.J. Hoyt, N. Provatas, J. Rottler, C.W. Sinclair, H.S. Zurob, Multi-scale modeling of phase transformations in steels, *JOM* 66 (5) (2014) 740–746, doi:[10.1007/s11837-014-0919-x](https://doi.org/10.1007/s11837-014-0919-x).
- [48] Z.X. Tian, J.X. Yan, W. Hao, W. Xiao, Effect of alloying additions on the hydrogen-induced grain boundary embrittlement in iron, *J. Phys.: Condens. Matter* 23 (1) (2010) 015501, doi:[10.1088/0953-8984/23/1/015501](https://doi.org/10.1088/0953-8984/23/1/015501).
- [49] S. Kim, S.-G. Kim, M.F. Horstemeyer, H. Rhee, The effects of Vanadium on the strength of a bcc Fe Σ3(111)[1–10] grain boundary, arXiv:1201.5915 [cond-mat] (2012).
- [50] C.J. McMahon, V. Vitek, G.R. Belton, On the theory of embrittlement of steels by segregated impurities, *Scr. Metall.* 12 (9) (1978) 785–789, doi:[10.1016/0036-9748\(78\)90036-4](https://doi.org/10.1016/0036-9748(78)90036-4).

- [51] C.L. Briant, On the chemistry of grain boundary segregation and grain boundary fracture, *Metall. Trans. A* 21 (9) (1990) 2339–2354, doi:[10.1007/BF02646981](https://doi.org/10.1007/BF02646981).
- [52] L. Huber, R. Hadian, B. Grabowski, J. Neugebauer, A machine learning approach to model solute grain boundary segregation, *npj Comput. Mater.* 4 (1) (2018) 1–8, doi:[10.1038/s41524-018-0122-7](https://doi.org/10.1038/s41524-018-0122-7).
- [53] D. Scheiber, L. Romaner, Impact of the segregation energy spectrum on the enthalpy and entropy of segregation, *Acta Mater.* 221 (2021) 117393, doi:[10.1016/j.actamat.2021.117393](https://doi.org/10.1016/j.actamat.2021.117393).
- [54] M. Wagih, P.M. Larsen, C.A. Schuh, Learning grain boundary segregation energy spectra in polycrystals, *Nat Commun* 11 (1) (2020) 6376, doi:[10.1038/s41467-020-20083-6](https://doi.org/10.1038/s41467-020-20083-6).
- [55] M. Wagih, C.A. Schuh, Grain boundary segregation beyond the dilute limit: separating the two contributions of site specificity and solute interactions, *Acta Mater.* 199 (2020) 63–72, doi:[10.1016/j.actamat.2020.08.022](https://doi.org/10.1016/j.actamat.2020.08.022).
- [56] T. Tanaka, Y. Gohda, Prediction of the Curie temperature considering the dependence of the phonon free energy on magnetic states, *npj Comput. Mater.* 6 (1) (2020) 1–7, doi:[10.1038/s41524-020-00458-5](https://doi.org/10.1038/s41524-020-00458-5).
- [57] K. Leitner, D. Scheiber, S. Jakob, S. Primig, H. Clemens, E. Povoden-Karadeniz, L. Romaner, How grain boundary chemistry controls the fracture mode of molybdenum, *Materials & Design* 142 (2018) 36–43, doi:[10.1016/j.matdes.2018.01.012](https://doi.org/10.1016/j.matdes.2018.01.012).